European Journal of Medicinal Chemistry 144 (2018) 164–178

Contents lists available at ScienceDirect

European Journal of Medicinal Chemistry

journal homepage: http://www.elsevier.com/locate/ejmech

Research paper

4-arylamidobenzyl substituted 5-bromomethylene-2(5*H*)-furanones for chronic bacterial infection

Xing-Jun Xu [a, 1], Fang Wang [a, b, 1], Ting Zeng [a], Jing Lin [a, *], Jun Liu [a], Yi-Qun Chang [a], Ping-Hua Sun [a], Wei-Min Chen [a, **]

[a] College of Pharmacy, Jinan University, Guangzhou, 510632, PR China
[b] Department of Scientific Research, Qingdao Stomatological Hospital, Qingdao, 266001, PR China

ARTICLE INFO

Article history:
Received 10 September 2017
Received in revised form
11 November 2017
Accepted 27 November 2017
Available online 2 December 2017

Keywords:
Chronic bacterial infections
Quorum sensing inhibitor
Anti-inflammation
PPARγ

ABSTRACT

Bacterial quorum-sensing (QS) can cause bacterial biofilm formation, thus induce antibiotic resistance and inflammation in chronic bacterial infections. A series of novel 4-arylamidobenzyl substituted 5-bromomethylene-2(5*H*)-furanones were designed by introducing of brominated furanones into rosiglitazone skeleton, and their potential application in the treatment of chronic bacterial infection was evaluated with regard to their disruption of quorum sensing and anti-inflammatory activities *in vitro* as well as in animal infection model. Compound **2e** displayed both potent QS inhibitory activity and anti-inflammatory activity. Further mechanism studies revealed that the biological effects of **2e** and **2k** could be attributed, at least in part, to their interaction with PPARγ, and consequent suppression of the activation of NF-κB and MAPK cascades. Importantly, pretreatment with **2e** significantly protects mice from lethal-dose LPS challenge. Thus, these data suggest that the dual effective derivative **2e** may serve as a valuable candidate for the treatment of chronic bacterial infection.

1. Introduction

The increasing prevalence of persistent chronic bacterial infections, such as venous leg ulcers, diabetic foot ulcers or medical device-related infection, which frequently lead to high morbidity and mortality [1,2], calls for the development of new therapeutic strategies. Chronic wounds often harbor bacterial infections, and bacterial resistance that caused by biofilm formation is rather common in chronic wound infections. In general, biofilm is an extracellular polymeric matrix consisting of proteins, lipids, uncleic acids and polysaccharides, which could protect bacteria from the host immune response and cause high intrinsic resistance (10–1000 fold higher tolerance) against various antibiotic agents and thus result in the extremely difficult to eradicate the chronic wound infections [3]. Quorum-sensing (QS) circuits, including *Las*, *Rhl*, and *Pqs* pathways are the core systems that responsible for the regulation of biofilm formation and virulence factors secretion in most gram-negative opportunistic pathogen, such as *Pseudomonas aeruginosa* (*P. aeruginosa*) [4].

On the other hand, it is well-known that bacterial endotoxin such as lipopolysaccharides (LPS), a component of the cell wall of gram-negative bacteria, as well as 3-oxododecanoyl homoserine lactone ($3OC_{12}$-HSL), a signaling compound in QS circuits, are the potent microbial initiators of inflammation [5]. Thus, long-term bacterial infection accompanied by biofilm often induces aggravated inflammation in host tissues that with chronic wound infections, and subsequently lead to chronic inflammatory responses and irreversible organ damage [6]. Consequently, anti-inflammation is also an important aspect for the treatment of chronic bacterial infections.

Accumulating studies have shown that substance with both QS inhibitory and anti-inflammatory effects could be effective in the treatment of chronic bacterial infections. LL-37, a human host defense peptide, which could modulate inflammatory responses by inhibiting the release of the proinflammatory cytokine tumor necrosis factor α (TNF-α) in LPS-stimulated human monocytic cells, and inhibit the formation of bacterial biofilms *in vitro*, was proved to be effective in enhancing healing of hard-to-heal venous leg ulcers. The clinical applicability of this rather large compound has already been demonstrated in a phase I and II clinical trial showing

* Corresponding author.
** Corresponding author.
E-mail addresses: linjing_jnu@163.com (J. Lin), twmchen@jnu.edu.cn (W.-M. Chen).
[1] These authors contributed equally.

https://doi.org/10.1016/j.ejmech.2017.11.085
0223-5234/

-promising results for topical treatment of patients with chronic leg ulcers [7–9]. Furthermore, treatment with honey, which was validated with both anti-microbial and anti-inflammatory activity [10–12], has presented significantly healing and contraction effects on burns [13,14]. Thus, development of compounds that with both QS inhibitory and anti-inflammatory activities may be an effective therapeutic strategy for the treatment of chronic bacterial infections.

It has been reported [15–18] that rosiglitazone, a well-known peroxisome proliferator-activated receptor γ (PPARγ) agonist, has shown significant anti-inflammatory properties because of its ability to activate PPARγ, and consequently to suppress nuclear factor κB (NF-κB), leading to an alteration in the expression of pro-inflammatory genes such as TNF-α and interleukin-6 (IL-6). Moreover, the proinflammatory effect of $3OC_{12}$-HSL, a singnalling compound in QS sircuits, in lung epithelial cells can be blocked by the PPARγ agonist rosiglitazone [19], Which suggests that rosiglitazone is likely to be a potential leading compound for the development of agents used in the treatment of inflammation caused by bacterial infections. Meanwhile, most QS systems of gram-negative bacteria employ *N*-acyl homoserine lactones (AHL) as the signaling molecular to control biofilm formation [16,17], and it has been reported that compounds bearing the AHL analogue moiety-halogenated furanone have excellent QS inhibitory activities [20]. Our previous work showed that compounds bearing a brominated furanone moiety have excellent QS inhibitory activity [21–23]. Based on the above facts, we hypothesized that introduction of brominated furanones into rosiglitazone by scaffold hopping strategy may lead to compounds potentially with both anti-inflammatory and QS inhibitory activity.

Therefore, in the present study, using a scaffold hopping strategy, a series of novel 4-arylamidobenzyl substituted 5-bromomethylene-2(5*H*)-furanones were designed by introducing of brominated furanones (QS inbibitory moiety) into rosiglitazone skeleton (anti-inflammatory agent) (Fig. 1), and their potential application in the treatment of chronic wound infection were evaluated with regard to their QS inhibitory and anti-inflammatory activities *in vitro* as well as in animal infection model. Western blot experiments and docking studies were also performed in an attempt to clarify the anti-inflammation mechanism.

2. Chemistry

Design of compounds. Scaffold hopping (also termed chemotype switching), a medicinal chemistry method for molecular backbone replacements, is an integral component of the drug discovery process and is an effective drug-design strategy for development of novel molecules with potent activity [24,25]. In this paper, in order to develop preferable agents for the treatment of chronic bacterial infections, molecular backbone replacements have been carried out by scaffold hopping with rosiglitazone. As shown in Fig. 1, the drug-design strategy involved: (a) the thiazolidinedione moiety of rosiglitazone being replaced by brominated furanyl group, which is an important pharmacophore with QS inhibitory activity that was identified in our earlier work [21–23]; (b) the section C being replayed with a substituted benzene ring or aromatic heterocyclic ring to increase the structural diversity of the compounds; (c) the section C and B being linked with an amide bond with the aim of improving the solubility of the compounds.

Synthesis of compounds. The synthesis of the designed compounds in Fig. 1 was accomplished as outlined in Scheme 1 (**1a-1m** and **2a-2m**). In general, the target compounds were obtained *via* a seven-step strategy. Firstly, the starting materials, benzylacetone and glyoxylic acid were converted into (*E*)-3-benzyl-4-oxopent-2-enoic acid (**1**) *via* the cross Aldol condensation in orthophosphoric acid [26]. Then, 3-benzyl-4-oxopentanoic acid (**2**) was prepared from the reaction of compound **1** with zinc dust as reducing agent in acetic acid. Compound **2** reacted with fuming nitric acid to yield 3-(4-nitrobenzyl)-4-oxo-pentan-oic acid (**3**) intermediates *via* a nitration reaction [27]. Bromination of compound **3** was easily accomplished, and the product was then reacted with phosphorus pentoxide to give the intermediate 5-(dibromomethylene)-4-(4-nitrobenzyl)furan-2(5*H*)-one (**4**) and (*Z*)-5-(bromomethylene)-4-(4-nitrobenzyl)furan-2(5*H*)-one (**5**) in dry dichloromethane [26,28]. The subsequent synthetic procedure typically involved the reduction of the nitro group to form the 4-(4-aminobenzyl)-5-(dibromomethylene)- furan-2(5*H*)-one (**6**) and (*Z*)-4-(4- aminobenzyl)-5-(bromomethylene)furan-2(5*H*)-one (**7**) using reduced iron powder and ammonium chloride in acetone under a nitrogen atmosphere [29,30]. Finally, compound **6** or **7** was connected with different acyl chloride derivatives *via* acylation with dry pyridine as base in dichloromethane to form the amide end-products [31,32] as shown in Scheme 1.

A notable problem from a chemical point of view was that *Z* and *E* geometrical isomers around the exocyclic double bond (CH=C) were possible in compounds **2a-2m**. The ^{1}H NMR spectrum of **2a-2m** had only one signal for the 5-(bromomethylene)furan-2-one proton showing that the chemical shifts were basically in the same range from 6.24 to 6.27 ppm for **2a**, **2h, 2i** (in deuterated dimethylsulfoxide solution) and from 6.06 to 6.14 ppm for **2b-2g**, **2j-2m** (in deuterated acetone solution). It has been reported that the chemical shift value for the exocyclic olefinic proton in 5-(bromomethylene)furan-2-ones are characteristic for either the (*Z*)-isomer (typically δ 6.24 ppm) or the (*E*)-isomer (typically δ 6.57 ppm) [33]. Additionally, the *Z*-configuration had been reported to be thermodynamically more stable than the *E*-

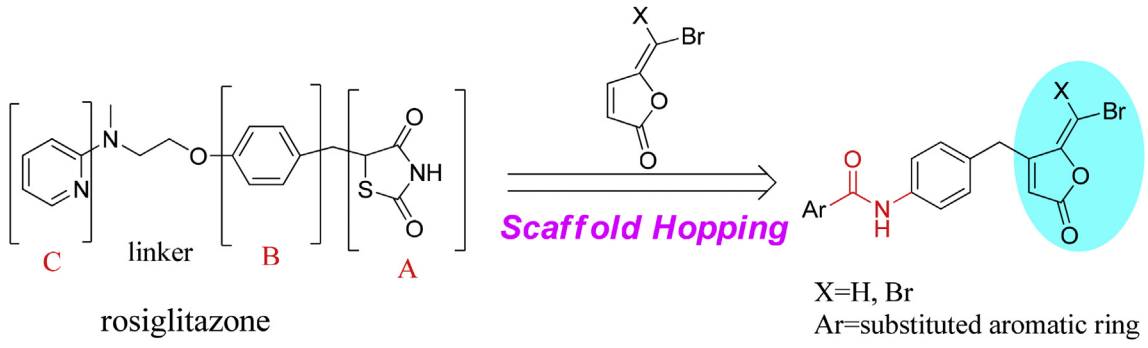

Fig. 1. Drug design by scaffold hopping strategy from rosiglitazone.

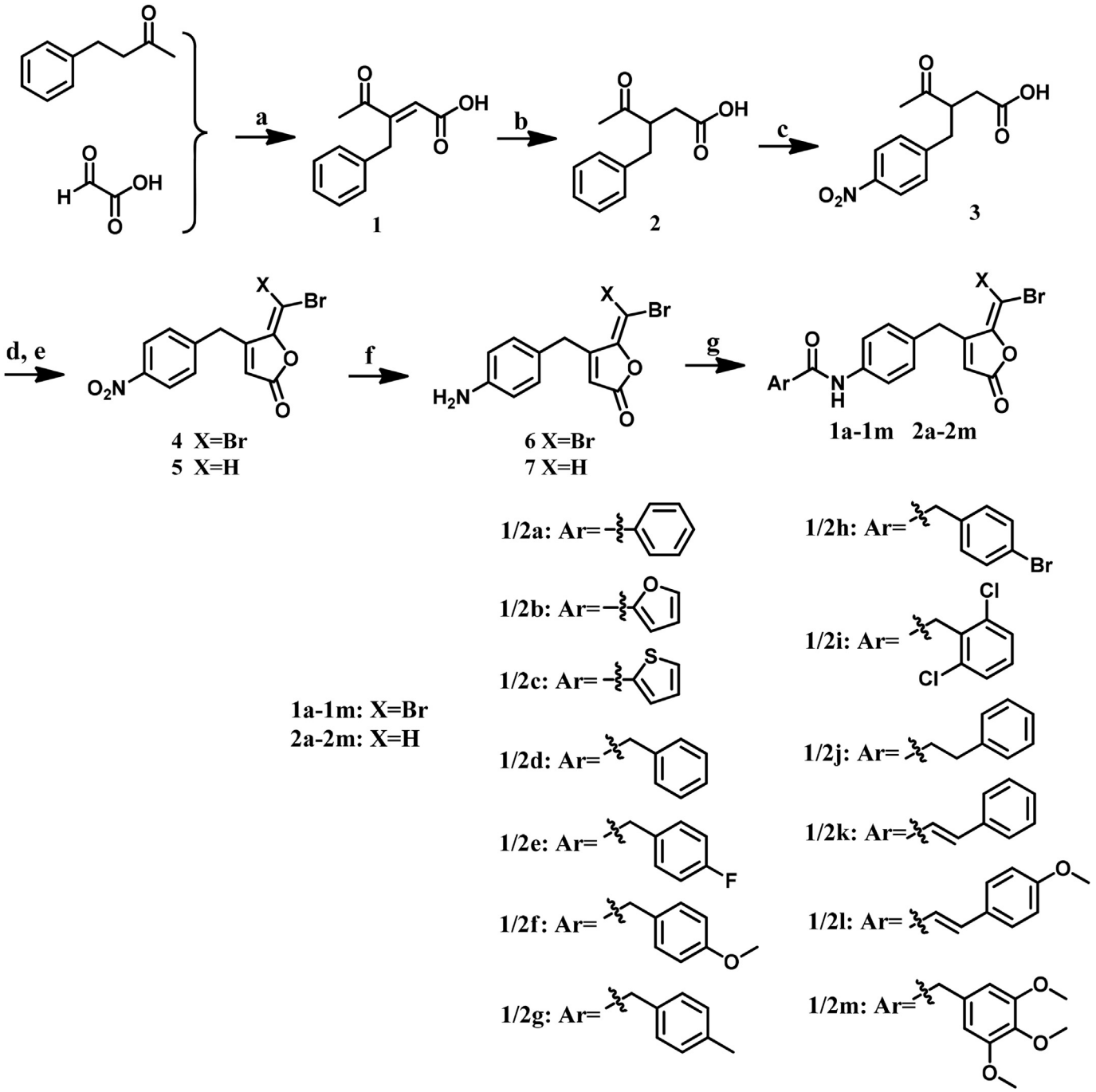

Scheme 1. General synthesis of compounds **1a-1m** and **2a-2m**$^{\triangle}$. $^{\triangle}$Reagents and conditions: (a) phosphoric acid, 85 °C, 4 h; (b) zinc dust, AcOH/H_2O, reflux; (c) fuming nitric acid, −20 °C; (d) Br_2, $CHCl_3$, reflux; (e) P_2O_5, DCM, reflux; (f) Fe, NH_4Cl, acetone/H_2O, reflux; (g) Et_3N, DCM, 0 °C to r.t.

configuration [34,35]. It is also important to note that the alkyl chain at C4 of 5-(bromomethylene)furan-2-one discourages formation of the transition state leading to the (*E*)-isomer, due to steric clashes with the exocyclic bromine atom. These results therefore suggest that the preferred configuration of synthesized compounds was the *Z* configuration.

All the synthesized compounds were fully analyzed and characterized by ^{1}H, ^{13}C nuclear magnetic resonance (NMR), mass spectrometry (MS) and high resolution mass spectrometry (HRMS) and HPLC purity analysis before beginning biological evaluation.

3. Results and discussion

Inhibition of Quorum Sensing Systems on *P. Aeruginosa*. It is becoming increasingly clear that control of bacterial quorum sensing development is a potential approach to reduce of biofilm associated antibiotic resistance and chronic inflammation occurring in infectious diseases [36]. In this paper, all of the designed compounds were consequently firstly evaluated for their QS inhibitory activity using QS monitors *lasB-gfp*, *rhlA-gfp*, and *pqsA-gfp* which can indicate the activity of the promoter of *lasB*, *rhlA*, and

pqsA gene based on expression of green fluorescence protein (GFP) in *P. aeruginosa* PAO1. At here, *P. aeruginosa*, which can cause a wide range of infections and inflammations through the formation of biofilm in a variety of hosts thus were chosen as the model strain [37]. The experiments were performed using a fixed concentration of 10 μM, and rosiglitazone and the brominated-2(5*H*)-furanone (Fig. 2) were taken as standard drugs.

As depicted in Table 1, the results of QS inhibitory activity reflexed by the *gfp* (ASV) expression levels in QS reporter strains showed that all the 4-arylamidobenzyl substituted 5-bromomethylene-2(5*H*)-furanones (**1a-1m** and **2a-2m**) almost exhibited an improved inhibitory effect on all the three QS systems of *P. aeruginosa* compared to that of the reference compound rosiglitazone. Notably, some newly synthesized compounds even showed a better QS inhibitory activity than the positive control agent brominated-2(5*H*)-furanone, especially for *pqs* system, in which, compounds **2e** and **2h** displayed promising QS inhibitory activities in *pqs* system, with the inhibition rates up to 50.29 ± 1.07% and 40.75 ± 6.42% respectively. Our results suggest that introduction of a halogenated furanone, *e.g.* a brominated furanone into the molecule would increase its QS inhibitory activity.

Inhibition of NO Production in (LPS)-Stimulated RAW264.7 Cells [38,39]. On the purpose of designing dual-effect molecular that with both QS inhibitory activity and anti-inflammatory effect to overcome chronic bacterial infection problems, next, the anti-inflammatory activity of all the synthesized compounds were therefore evaluated for their inhibitory activity against lipopolysaccharide (LPS)-induced nitric oxide (NO) release in RAW264.7 cells for NO has been widely recognized as a ubiquitous pro-inflammatory mediator that plays key roles in various inflammation-associated diseases. The macrophages were pre-treated with compounds for 2 h, then LPS was added and the system was incubated for 48 h. The amount of NO was determined by the Griess method. Rosiglitazone and indomethacin (Fig. 2) were taken as standard drugs for anti-inflammation studies.

As depicted in Table 2, most of the 4-arylamidobenzyl substituted 5-bromomethylene-2(5*H*)-furanones (**1a-1m** and **2a-2m**) displayed improved NO inhibitory activity compared to rosiglitazone and indomethacin. In particular, compounds **2e** and **2k** demonstrated a reasonably good anti-inflammatory activity at a concentration of 10 μM. Their NO inhibition rates were 73.7 ± 3.3% and 70.0 ± 3.5%, respectively.

Based on these results, some preliminary structure-activity relationships (SAR) of the 4-arylamidobenzyl substituted 5-bromomethylene-2(5*H*)-furanones can be summarized: (a) the 4-benzyl-5-monobromomethylene-furan-2(5*H*)-one structure is conducive to improvement of anti-inflammatory activity (**2a-2m** compared to **1a-1m**, for example, **2a** compared to **1a**); (b) the anti-inflammatory activity increases gradually with an increase of the length of carbon chain between the ring B and ring C (Fig. 1), and a two-atom linker could be the most favorable (**2j** compared to **2d** and **2a**). Moreover, the introduction of a double bond increased the activity further (**2k** compared to **2j**); (c) if C ring is substituted with a heterocyclic ring rather than a benzene ring, the anti-inflammatory effect is better (**2b** and **2c** compared to **2a**); (d) electron-withdrawing substituents (fluorine, chlorine or bromine) in the phenyl ring C would increase the NO inhibitory activity, and introduction of fluorine led to the best activity (**2e**, **2h** and **2i**

Table 1
Inhibition rates of the synthesized compounds to the expression of *gfp*(ASV) in PAO1-*lasB-gfp*, PAO1-*rhlA-gfp*, and PAO1-*pqsA-gfp* reporter strains.

Compound	PAO1-*lasB-gfp*	PAO1-*rhlA-gfp*	PAO1-*pqsA-gfp*
Fura[a]	21.43 ± 2.55*	24.03 ± 1.08*	20.19 ± 3.03*
Rosi[b]	7.43 ± 1.40	15.51 ± 0.07	9.19 ± 0.24
1a	21.19 ± 0.41*	20.25 ± 4.34*	28.23 ± 0.87**
2a	16.13 ± 0.40	17.20 ± 2.47	34.54 ± 3.20**
1b	22.89 ± 0.31*	23.57 ± 4.57*	34.64 ± 4.04**
2b	17.33 ± 0.81	13.64 ± 2.48	20.37 ± 3.21*
1c	19.97 ± 5.04*	19.57 ± 3.65	26.44 ± 1.91**
2c	10.22 ± 0.92	23.93 ± 2.20*	20.33 ± 1.02*
1d	19.21 ± 1.01*	19.22 ± 2.93*	24.83 ± 2.00*
2d	18.01 ± 2.92*	17.28 ± 1.82	25.82 ± 1.72**
1e	9.49 ± 3.29	15.93 ± 0.92	19.99 ± 3.01
2e	15.20 ± 2.05	14.71 ± 4.97	50.29 ± 1.07**
1f	11.76 ± 2.29	13.77 ± 4.27	20.55 ± 1.15*
2f	14.75 ± 0.37	11.81 ± 3.49	26.44 ± 1.91**
1g	14.22 ± 0.47	16.37 ± 3.30	24.50 ± 2.86*
2g	19.02 ± 4.92*	18.22 ± 3.92*	29.83 ± 1.02**
2h	10.41 ± 2.38	20.01 ± 2.49*	27.92 ± 2.93**
2h	24.87 ± 4.61*	17.17 ± 3.87	40.75 ± 6.42**
1i	19.13 ± 2.49*	19.20 ± 2.30*	19.29 ± 2.29*
2i	16.91 ± 4.51	15.17 ± 2.88	17.62 ± 2.53
1j	11.01 ± 3.21	19.50 ± 2.63*	22.89 ± 0.25*
2j	14.94 ± 0.01	15.25 ± 3.61	20.60 ± 1.20*
1k	9.48 ± 5.47	18.07 ± 7.62*	16.22 ± 0.19
2k	11.84 ± 4.32	12.02 ± 1.09	23.09 ± 1.44*
1l	5.03 ± 0.92	12.93 ± 1.48	21.92 ± 3.99*
2l	12.23 ± 6.66	10.56 ± 2.01	24.30 ± 1.17*
1m	9.79 ± 1.17	7.66 ± 5.99	19.53 ± 3.11*
2m	8.53 ± 0.79	5.57 ± 3.44	20.28 ± 2.37*

**P < 0.01, *P < 0.05 versus the blank (cultured with bacteria only) group.
Results are shown as means ± SD (n = 3) of three independent experiments.
[a] Fura: brominated-2(5*H*)-furanone.
[b] Rosi: rosiglitazone.

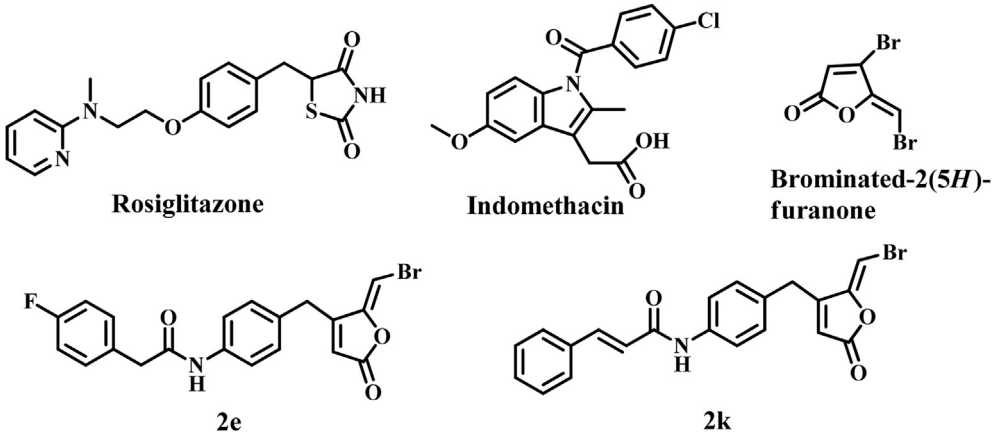

Fig. 2. Structures of rosiglitazone, indomethacin, brominated-2(5*H*)-furanone, **2e** and **2k**.

Table 2
The inhibitory effects of the synthesized compounds on NO production in LPS-stimulated RAW264.7 cells.

Compounds	NO inhibition (%)[a]	Compounds	NO inhibition (%)[a]
Rosi[b]	16.6 ± 3.8**	Indo[c]	29.4 ± 4.7**
1a	30.3 ± 3.7**	**2a**	46.2 ± 2.9**
1b	44.5 ± 9.1**	**2b**	59.9 ± 5.8**
1c	39.9 ± 6.6**	**2c**	54.2 ± 4.3**
1d	44.1 ± 2.9**	**2d**	59.5 ± 3.7**
1e	59.2 ± 3.7**	**2e**	73.7 ± 3.3**
1f	25.2 ± 3.6**	**2f**	39.3 ± 4.2**
1g	19.0 ± 3.7**	**2g**	29.4 ± 5.0**
1h	50.7 ± 2.9**	**2h**	64.9 ± 3.0**
1i	53.5 ± 3.3**	**2i**	66.6 ± 3.8**
1j	48.1 ± 4.6**	**2j**	64.8 ± 5.2**
1k	54.4 ± 4.3**	**2k**	70.0 ± 3.5**
1l	44.3 ± 6.4**	**2l**	61.0 ± 5.3**
1m	21.2 ± 1.8**	**2m**	34.3 ± 2.7**

**P < 0.01.
*P < 0.05 versus the LPS (treated with LPS only) group.
[a] Results were showed as means ± SD (n = 4) of at least three independent experiments.
[b] Rosi: rosiglitazone.
[c] Indo: indomethacin.

compared to **2d**); (e) an electron-donating substituent (methyl or methoxyl) in the phenyl ring C decreases it's NO inhibitory activity (**2f**, **2g** and **2m** compared to **2d**). Consequently, these results will be useful in the future to guide the design and modification of new anti-inflammatory agents.

Cytotoxicity in RAW264.7 Cells. To investigate whether the effects of **2e** and **2k** on suppression of the production of NO were related to cell viability, these compounds were further exposed to RAW264.7 macrophages to explore their cytotoxicity using a methyl thiazolyl tetrazolium (MTT) assay. The results of the cytotoxicity assay are shown in Table 3 and clearly indicate that all the agents (rosiglitazone, indomethacin, **2e**, **2k**, GW9662 and LPS) at the concentrations measured here had no obvious cytotoxicity, and the relative cell viabilities of the treated cells were all more than 95%. The NO inhibitory effects of **2e** and **2k** could probably be attributed to the interaction of these two compounds with their specific target. Accordingly, on the basis of cellular viability *in vitro*, these non-toxic concentrations were used and evaluated in the following experimental processes.

Inhibition of TNF-α and IL-6 Production in RAW264.7 Cells. TNF-α and IL-6 are two crucial pro-inflammatory mediators, their blockers are recognized as effective agents for the treatment of inflammatory disease [40,41]. The ability of an agent to inhibit the LPS-induced increases in TNF-α and IL-6 production is an important criterion with which to assess the potential anti-inflammatory effects of drug candidates [42]. Consequently, the anti-inflammatory effects of compounds **2e** and **2k** that showed significant NO inhibitory activities were further confirmed by evaluating their *in vitro* TNF-α and IL-6 inhibitory effects using TNF-α and IL-6 specific enzyme linked immunosorbent assay (ELISA) experiment in LPS-induced RAW264.7 cells. Rosiglitazone and indomethacin (Fig. 2) were used as positive reference drugs. In the current study, both these two experiments were performed using a fixed concentration of 10 μM and in a time-dependent manner.

The results are shown in Table 4 and Fig. 3. It was shown that **2e** and **2k** induce a significant decrease in both the LPS-induced production of TNF-α and IL-6, while the positive control drugs exhibited evidently weaker inhibitory effects on either TNF-α or IL-6 production compared with those of **2e** and **2k** at all three detection times. For example, without treatment, after induction by LPS for 24 h, the concentration of TNF-α in RAW264.7 cells was 24216.0 ± 498.7 pg/mL, while the concentration of TNF-α was decreased to 18322.0 ± 241.6 pg/mL ($p < 0.01$) and 19550.0 ± 292.1 pg/mL ($p < 0.01$) respectively in **2e** and **2k** pre-treated RAW264.7 cells. These concentrations were evidently lower than those in cells pre-treated with the standard drugs rosiglitazone and indomethacin, whose TNF-α levels were 22226.0 ± 588.0 pg/mL ($p < 0.05$) and 20772.0 ± 558.9 pg/mL ($p < 0.01$), respectively (all p values vs. LPS alone, 24216.0 ± 498.7 pg/mL). Moreover, the experimental data show that **2e** and **2k** also possess remarkable inhibitory activity on LPS-induced IL-6 production and on TNF-α production. As shown in Table 4, rosiglitazone and indomethacin inhibited IL-6 production from 407.6 ± 16.7 pg/mL (LPS alone) to 345.6 ± 25.6 pg/mL ($p < 0.05$) and 286.6 ± 19.5 pg/mL ($p < 0.01$) respectively at 24 h, while **2e** and **2k** induced a decrease in IL-6 production to the concentration of 145.2 ± 16.6 pg/mL ($p < 0.01$) and 158.2 ± 19.1 pg/mL ($p < 0.01$), respectively (all p values vs. LPS alone, 407.6 ± 16.7 pg/mL). From the above results, it becomes increasingly clear that **2k**, and especially **2e**, are excellent anti-inflammatory agents, which prompted us to investigate the possible anti-inflammatory mechanism of **2e** and **2k** by analyzing inflammatory-associated signaling pathways.

Western Blot Analysis for Interpretation of Possible Mechanisms. NF-κB pathway is an important signaling pathway associated with the process of inflammation [43]. Generally, LPS-induced

Table 3
Effects of compounds on the viability of RAW264.7 cells.

Compounds	Concentrations	Cell viability (%)[a]
Rosi[b]	10 μM	99.0 ± 6.9
Indo[c]	10 μM	100.8 ± 7.5
2e	10 μM	97.0 ± 4.6
2k	10 μM	103.7 ± 5.0
GW9662	5 μM	99.1 ± 6.3
LPS	500 ng/mL	99.4 ± 4.7
LPS	100 ng/mL	103.6 ± 3.0

[a] Results were expressed as means ± SD (n = 4) of three independent experiments.
[b] Rosi: rosiglitazone.
[c] Indo: indomethacin.

Table 4
The inhibitory effects of rosiglitazone, indomethacin, **2e** and **2k** on LPS-induced TNF-α and IL-6 production in RAW264.7 cells.

Compounds	TNF−α (pg/mL)[a]		
	6 h	12 h	24 h
Blank	135.3 ± 20.1	174.7 ± 37.8	238.0 ± 45.4
LPS	11922.0 ± 628.4##	21561.3 ± 857.0##	24216.0 ± 498.7##
LPS + Rosi[b]	11311.3 ± 823.0	20616.0 ± 655.7	22226.0 ± 588.0*
LPS + Indo[c]	10850.0 ± 691.5	19664.0 ± 576.1*	20772.0 ± 558.9**
LPS+**2e**	7524.7 ± 50.6**	13362.7 ± 129.4**	18322.0 ± 241.6**
LPS+**2k**	7750.0 ± 89.4**	15037.3 ± 1033.9**	19550.0 ± 292.1**
	IL-6 (pg/mL)[a]		
	6 h	12 h	24 h
Blank	1.2 ± 0.3	1.7 ± 0.2	3.1 ± 1.1
LPS	94.6 ± 5.9##	175.2 ± 10.2##	407.6 ± 16.7##
LPS + Rosi[b]	64.8 ± 4.2**	140.0 ± 6.2**	345.6 ± 25.6*
LPS + Indo[c]	59.6 ± 6.1**	120.7 ± 2.7**	286.6 ± 19.5**
LPS+**2e**	17.0 ± 1.2**	66.3 ± 17.8**	145.2 ± 16.6**
LPS+**2k**	19.6 ± 1.7**	75.3 ± 20.3**	158.2 ± 19.1**

##P < 0.01.
#P < 0.05 versus the blank (cultured with fresh medium only) group.
**P < 0.01.
*P < 0.05 versus the LPS (treated with LPS only) group.
[a] Results were showed as means ± SD (n = 3) of three independent experiments.
[b] Rosi: rosiglitazone.
[c] Indo: indomethacin.

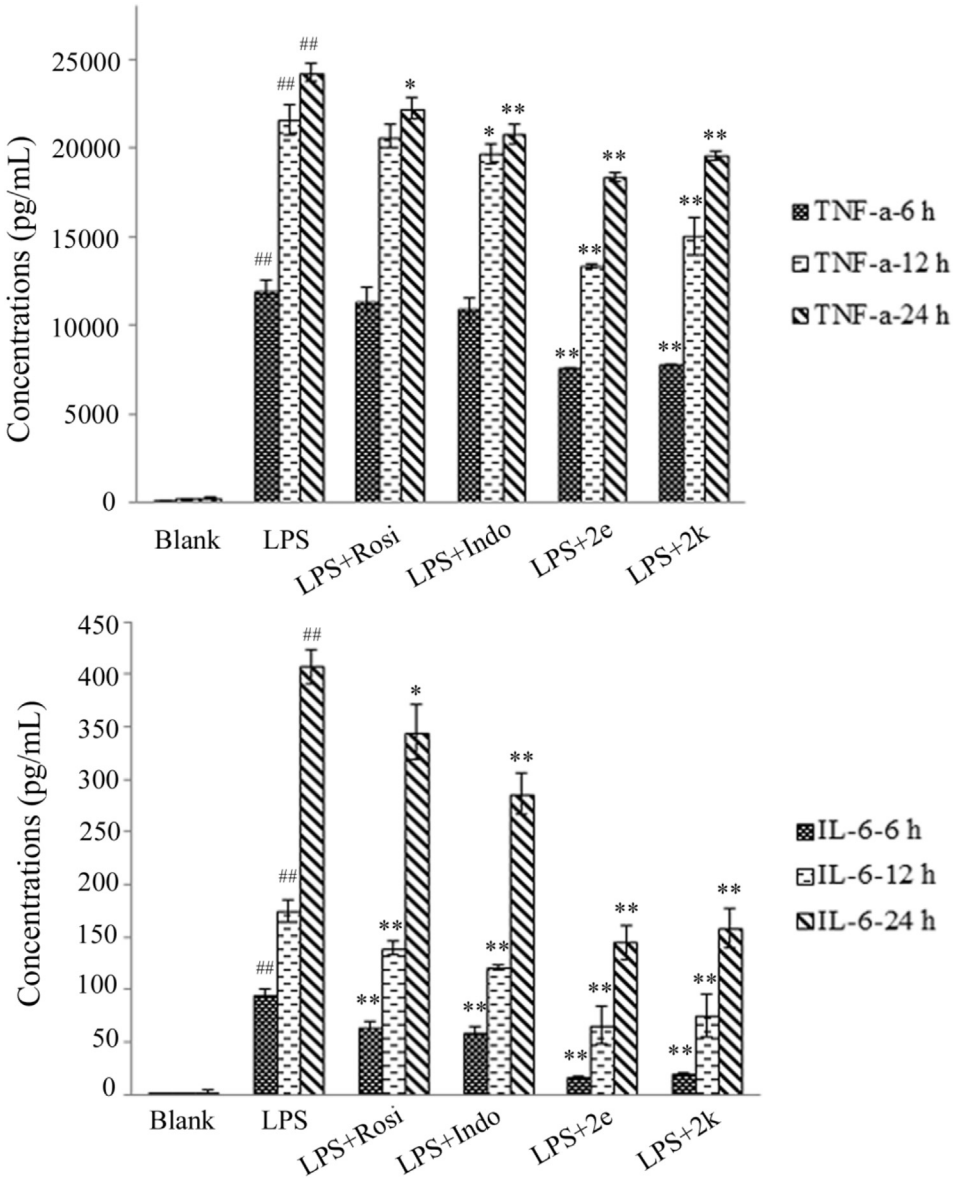

Fig. 3. The effects of rosiglitazone, indomethacin, **2e** and **2k** on the LPS-induced production of TNF-α and IL-6 in RAW264.7 cells. RAW264.7 cells were treated with rosiglitazone (10 μM), indomethacin (10 μM), **2e** (10 μM) and **2k** (10 μM) and LPS (100 ng/mL) for 6 h, 12 h and 24 h. Data are presented as means ± SD (n = 3). $^{\#\#}P < 0.01$, $^{\#}P < 0.05$ versus the blank (cultured with fresh medium only) group; $^{**}P < 0.01$, $^{*}P < 0.05$ *versus* the LPS (treated with LPS only) group.

activation of NF-κB pathway involving phosphorylation of inhibitor kappa B alpha (IκB-α) kinase, and subsequently ubiquitination and degradation of IκB-α, as well as the phosphorylation of NF-κB p65, plays a key regulatory role in the occurrence of inflammation [44–46]. Meanwhile, the activation of MAPK pathways which mainly involve extracellular regulated protein kinases (ERK1/2, or p42/44) and p38 MAPK is also often observed in LPS-stimulated macrophages. It is well accepted that the up-regulation of the synthesis of inflammatory mediators induced by LPS, involves NF-κB and MAPK activation, and is modulated by PPARγ, and the MAPK and NF-κB activation can be inhibited by pre-treatment with PPARγ activator, such as rosiglitazone [47–51]. Therefore, in the present study, to determine whether the anti-inflammatory effects of **2e** and **2k** are associated with the PPARγ mediated activation of NF-κB and MAPK as leading compound rosiglitazone, the expression levels of these two pathways related proteins in RAW264.7 cells, with and without treatments by **2e** or **2k** were analyzed.

As shown in Fig. 4, phosphorylation of NF-κB p65, IκBα, ERK1/2 and p38 MAPK was significantly increased by treatment with LPS, which is commonly used as a pro-inflammatory stimulus, and the levels of the phosphorylation forms of these proteins decreased in varying degrees by treatment with **2e** and **2k**. Specifically, we found that **2k**, and especially **2e** significantly inhibits the phosphorylation of NF-κB p65, IκBα, ERK1/2 and p38 MAPK protein expression when compared with LPS-induced macrophages, while **2e** and **2k** had a slightly antagonistic effect on phosphorylation of IκBα. Additionally, to determine whether PPARγ participates in the influence of the phosphorylation of these proteins, a highly selective and irreversible PPARγ antagonist GW9662 [52], was used prior to treatment with **2e** or **2k**. Application of GW9662 (5 μM) can reverse the suppressive effects of **2e** and **2k** on the protein phosphorylations, which suggests that PPARγ plays a role in the regulation of phosphorylation of related proteins.

In view of these findings, it may be speculated that anti-

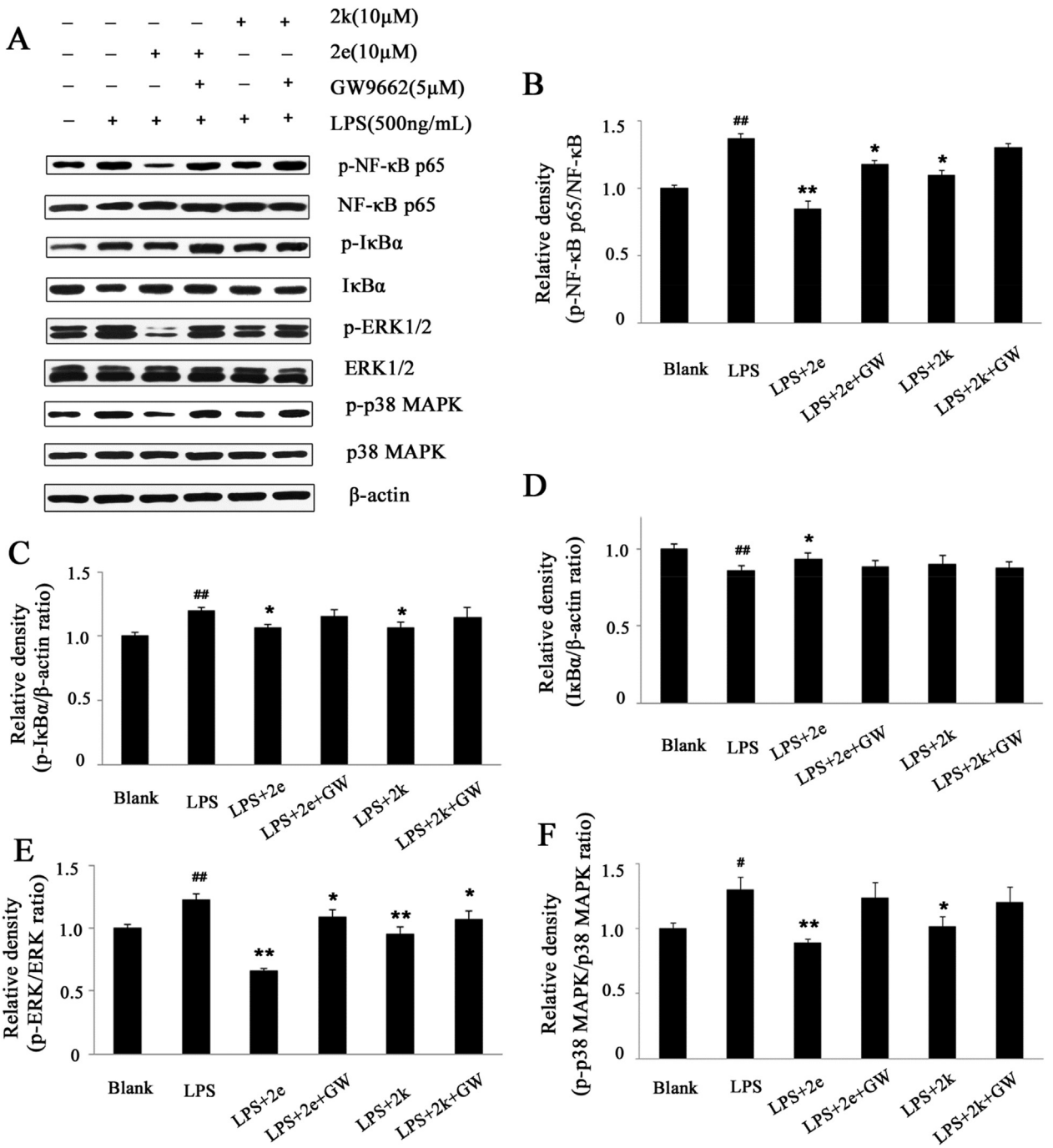

Fig. 4. The effects of compounds **2e** and **2k** on a LPS-induced phosphorylation of NF-κB p65, IκBα, ERK1/2 and p38 MAPK in RAW264.7 cells. RAW264.7 cells were treated with **2e** (10 μM), **2k** (10 μM), GW9662 (5 μM), and LPS (500 ng/mL) for 4 h. The levels of NF-κB p65, IκBα, ERK1/2, and p38 MAPK proteins, and their phosphorylated forms were analyzed using western blotting. Data are presented as means ± SD (n = 3). $^{\#\#}P < 0.01$, $^{\#}P < 0.05$ versus the blank (cultured with fresh medium only) group; $^{**}P < 0.01$, $^{*}P < 0.05$ versus the LPS (treated with LPS only) group.

inflammatory effects of **2e** and **2k** were due at least in part, to their interaction with PPARγ, thereby suppressing activation of the NF-κB and MAPK cascades, and leading to NO, TNF-α and IL-6 levels being decreased in LPS-stimulated RAW264.7 macrophages. Nonetheless, further studies are needed to confirm this conjecture.

Docking Analysis. To confirm the above speculation that **2e** and **2k** were likely to act as PPARγ agonists, docking studies were performed using the SYBYL 8.1 (Tripos, Inc., St. Louis, MO, USA) program package to investigate the interaction of **2e** and **2k** with PPARγ. Here, rosiglitazone and indomethacin, which are two known PPARγ activators, were used as reference molecules. The structure information of PPARγ protein used in the docking studies was obtained from the Protein Data Bank (PDB ID: 2PRG). Table 5 showed the docking scores of the four tested molecules with PPARγ.

Interestingly, the docking scores correlated well with the pharmacological testing results, the compounds **2e** and **2k** showing high docking scores with PPARγ, even higher than those for rosiglitazone and indomethacin. These results imply the possibility of the direct interaction of **2e** and **2k** with PPARγ. Furthermore, the

Table 5
Docking scores for the combination of rosiglitazone, indomethacin, **2e** and **2k** to PPARγ.

Compounds	Rosi[a]	Indo[b]	2e	2 k
Scores	6.94	4.92	7.96	7.71

[a] Rosi: rosiglitazone.
[b] Indo: indomethacin.

MOLCAD (Molecular Computer Aided Design) program was employed to visualize the binding mode between rosiglitazone, indomethacin, **2e** and **2k** and the PPARγ pocket. Fig. 5 displayed the MOLCAD cavity depth (CD) potential surfaces structure between the PPARγ-binding pocket and four compounds. The cavity depth color ramp ranged from blue (low depth values = outside of the pocket) to orange (high depth values = cavities deep inside the pocket). Fig. 6 shows the hydrogen bonding of these four compounds with PPARγ, and the hydrogen bonds are showing as dark dashed lines.

As shown in Fig. 5, four ligands are able to bind to PPARγ at different depths. Rosiglitazone and indomethacin were mostly located in a blue region, which indicates a relatively low depth, while compounds **2e** and **2k** were in a light yellow region with good flexibility, which revealed that the majority parts of these two molecules were anchored deep inside the pocket. In addition, as shown in Fig. 6, several strong hydrogen bonds were formed between **2e**, **2k** and PPARγ. Compound **2e** formed H-bonds with the imino groups of residues Ser289 and Arg288, and **2k** formed H-bonds with the Cys285 and Ser342 residues.

Taken together, the docking studies highlighted the binding modes between **2e**, **2k** and PPARγ, which reveals the strong binding ability of **2e** and **2k** to PPARγ, and provides strong evidence for the assumption that PPARγ was at least one of the specific targets of **2e** and **2k**.

Pretreatment with 2e Protects Mice from Lethal-Dose LPS Challenge. Before the animal experiment, compounds **2e** and **2k,** which exhibit the best anti-inflammatory activity were evaluated the growth effect of **2e** and **2k** on *P. aeruginosa* strain PAO1. Just as we expected, **2e** and **2k** would not affect the growth of bacteria, even at 100 μM Fig. 7 (A B). It means that our compounds may hardly emerge tolerance since it will not threaten germs' living. We further explored by a dose-dependent assay for their QS inhibitory activities used the most effected QS system-*pqs*. As shown in Fig. 7(C D), in line with the screening results, **2e** displayed excellent inhibitory activity on the expression of *pqs-gfp* in a concentration dependent manner, while **2k** almost has no effect on QS system. Therefore, **2e** with both good QS inhibitory activity and anti-inflammatory activity was forward to next animal model evaluation. In this study, the mouse model of LPS-injection-induced sepsis shock [53,54] was employed to determine whether **2e** can be able to attenuate endotoxin shock through inhibition of LPS-induced inflammatory response. Mice were daily treated with rosiglitazone or **2e** or LPS. On day 5, LPS (40 mg/kg) was intravenously intraperitoneally injected 1 h after the last administration. Survival rates are shown in Fig. 8. LPS (40 mg/kg) administration resulted in the death rate of 82% within one day, and death of all the mice in the model group within 2 days. In the positive group, administration of rosiglitazone (20 mg/kg, 1 mg/kg) shows the 45.5% and 36.5% survival rate on day 7. Similarly, administration of **2e** (high dose: 20 mg/kg and low dose: 5 mg/kg) also significantly improved

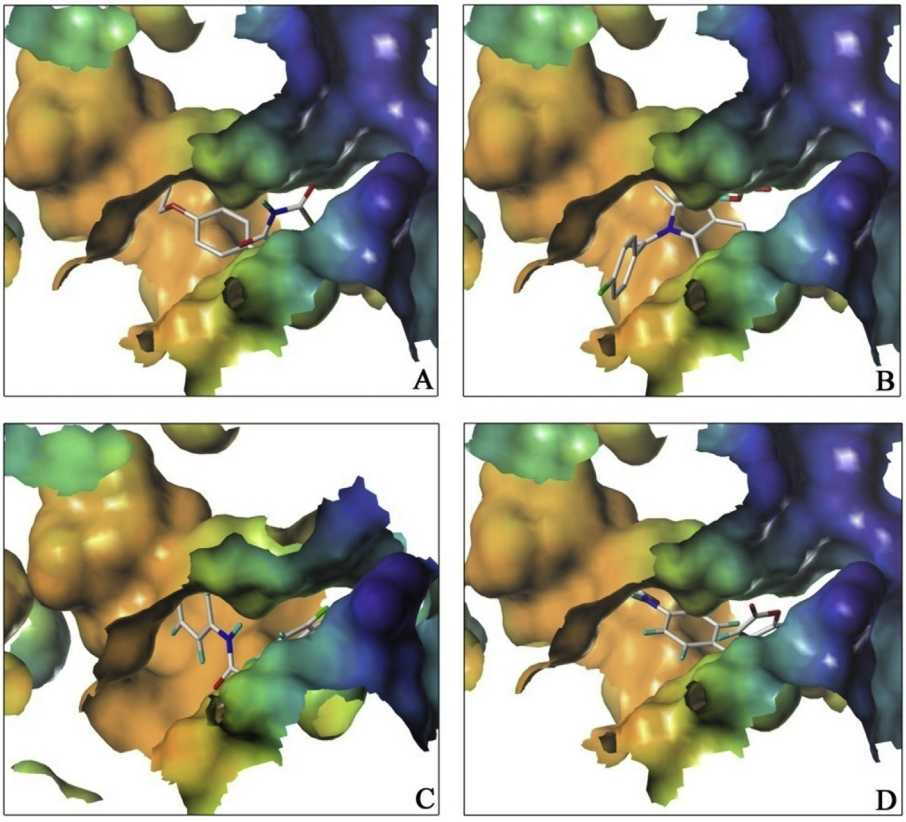

Fig. 5. The MOLCAD Multi-Channel surface structures displayed with cavity depth of the PPARγ within the (A) rosiglitazone, (B) indomethacin, (C) **2e** and (D) **2k**. The color ramp for cavity depth ranged from blue (outside of the pocket; most negative) to orange (deep inside the pocket; most positive).

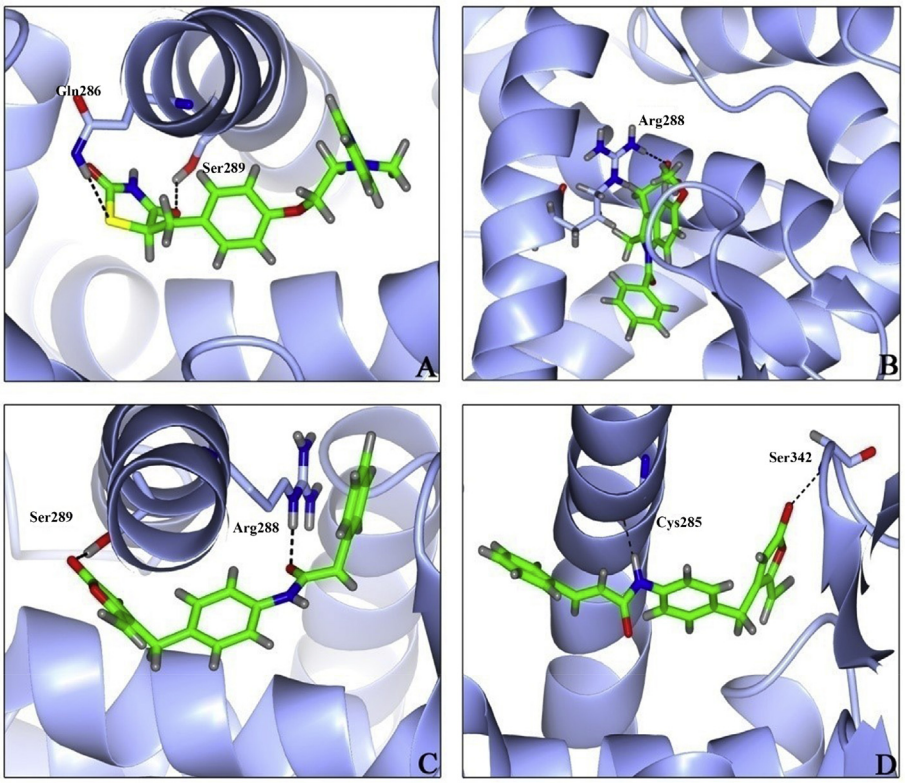

Fig. 6. Hydrogen bonds formed between PPARγ and (A) rosiglitazone, (B) indomethacin, (C) **2e** and (D) **2k**. Hydrogen bonds (HB) are shown as dark dashed lines. Hydrogen atoms are omitted for clarity.

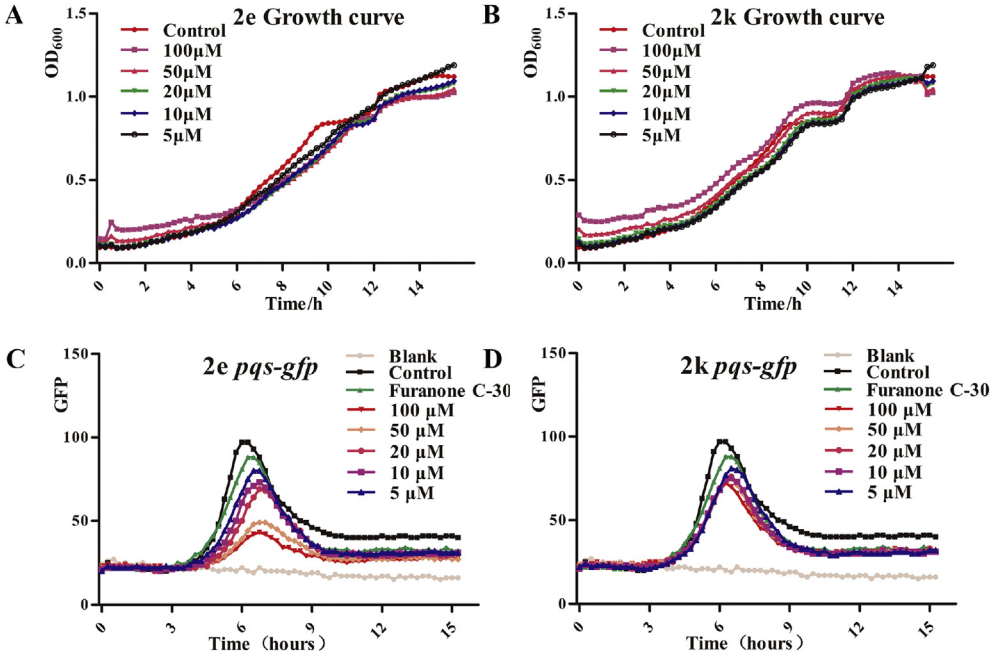

Fig. 7. (A) (B) Growth curves of compound **2e** and **2k** incubated with the PAO1, **(C) (D)** Dose-dependent inhibition curves of compound **2e** and **2k** incubated with the QS monitors PAO1-*pqsA-gfp*.

the survival rate of the LPS-injected mice (45.5% and 36.5% survival on day 7 in high dose group and in low dose group, respectively, $P < 0.05$ in both groups vs. LPS group). Thus, pretreated with **2e** can prolong survival in LPS-induced acute inflammatory.

4. Conclusion

In this study, a series of novel 4-arylamidobenzyl substituted 5-bromomethylene- 2(5*H*)-furanones have been designed and

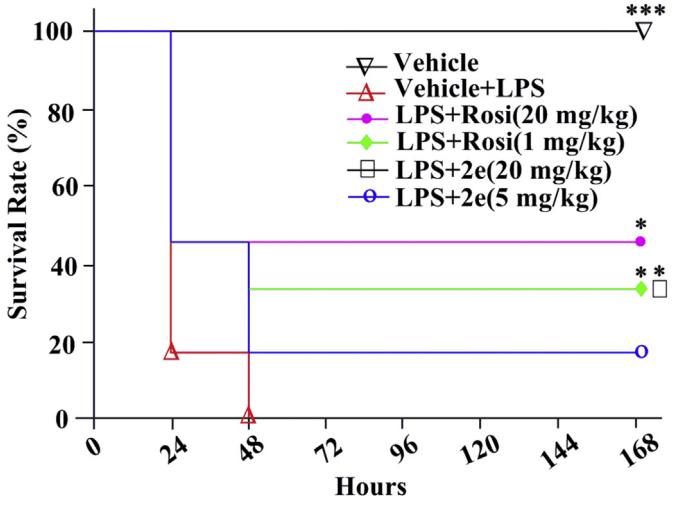

Fig. 8. Effects of **2e** on the mortality of mouse model of LPS-induced sepsis shock. Survival was recorded for 7 days after LPS injection at an interval of 12 h. n = 11 animals in each group. * means $p < 0.05$ vs LPS group, and ***means $p < 0.001$ vs LPS group.

synthesized based on rosiglitazone by scaffold hopping strategy, and their QS inhibitory and anti-inflammatory activities were evaluated. Among these compounds, a promising leading compound (**2e**) that not only shown potent QS inhibitory activity, but also excellent anti-inflammatory activity was identified. Furthermore, western blot and docking results revealed that the anti-inflammatory activity of this type of compound could also be attributed at least in part, to their interaction with PPARγ, thereby suppressing activation of NF-κB and MAPK cascades and leading to the decrease of NO, TNF-α and IL-6 levels in LPS-stimulated RAW264.7 macrophages. This study provides a valuable candidate **2e,** which could serve as a potential agent for the treatment of chronic bacterial infection. Meanwhile, these results revealed that a combination of the structural features with quorum sensing inhibitory activity into the potential anti-inflammatory agents are likely to be a valuable strategy to obtain drugs with both quorum sensing inhibitory and anti-inflammatory effects which induced by the chronic bacterial infections.

5. Experimental section

General Chemistry. All reagents and solvents were purchased in analytical grade from commercial suppliers. Flash column chromatography was carried out on silica gel obtained from Qindao Haiyang Chem. Solvents used including petroleum ether, EtOAc, DCM, MeOH, and $CHCl_3$ were purified and redistilled. ^1H NMR and ^{13}C NMR spectra were recorded on a Bruker Avance DPX300 (300 M) spectrometer with TMS as the baseline and were determined in DMSO-d_6 and acetone-d_6 solvent peaks as the internal reference. Chemical shifts are reported in parts per million (ppm) relative to the reference signal, and coupling constant (J) values are reported in hertz (Hz). Melting points were measured on an Optimelt automated melting point system and are uncorrected. Thin layer chromatography (TLC) was performed on precoated silica gel plates, and spots were visualized with UV light or potassium permanganate coloration. High-resolution mass spectra (HRMS) were recorded on an Agilent TOF/MS instrument equipped with an ESI interface. Detailed characterization data for the synthesized compounds are available in the supporting information of this manuscript.

Procedure for Synthesis of (*E*)-3-benzyl-4-oxopent-2-enoic acid (1). Glyoxylic acid (15.5 g, 0.21 mol) and benzylacetone (94.4 mL, 0.63 mol) were added to orthophosphoric acid (30 mL). The mixture was heated at 85 °C for 4 h and then stirred at room temperature overnight. Water (30 mL) was added to the mixture which was extracted with EtOAc (3 × 100 mL). The combined organic layer was washed with H_2O and brine, dried over anhydrous Na_2SO_4 and evaporated to give dark brown oil. The crude product was chromatographed on a silica gel column using petroleum ether/EtOAc/AcOH (5:1:0.03). Final product **1** was obtained as a pale yellow oil (22.3 g, 52.1%). ^1H NMR (300 MHz, acetone-d_6) δ 7.35 (d, J = 4.4 Hz, 4H), 7.30–7.16 (m, 1H), 6.94 (s, 1H), 4.28 (s, 2H), 2.47 (s, 3H). ^{13}C NMR (75 MHz, acetone-d_6) δ 200.8, 168.3, 153.6, 140.5, 130.4, 129.9, 128.7, 127.7, 32.9, 27.7. HRMS (ESI^+) calcd for $C_{12}H_{13}O_3$ $[M+1]^+$ 205.0859, found 205.0854.

Procedure for Synthesis of 3-benzyl-4-oxopentanoic acid (2). (*E*)-3-Benzyl-4-oxopent-2-enoic acid (**1**) (22.3 g, 0.16 mol) was dissolved in AcOH (200 mL) and H_2O (7.5 mL) mixture. Zinc dust (21.0 g, 0.32 mol) was added to the mixture slowly, then the mixture was heated to reflux and kept at this temperature for 2 h. The mixture was filtered with a sand core funnel. Water (200 mL) was added to the filtrate and the mixture was extracted with DCM (3 × 150 mL). The combined DCM phase was washed to neutral, dried over anhydrous Na_2SO_4 and evaporated under reduced pressure to give a brown oil (32.5 g, 97.9%). ^1H NMR (300 MHz, acetone-d_6) δ 10.52 (s, 1H), δ 7.39–7.13 (m, 5H), 3.25 (m, 1H), 2.95 (dd, J = 13.4, 6.8 Hz, 1H), 2.65 (dd, J = 13.9, 7.7 Hz, 2H), 2.34 (dd, J = 17.2, 4.3 Hz, 1H), 2.07 (s, 3H). ^{13}C NMR (75 MHz, acetone-d_6) δ 209.7, 173.2, 139.5, 129.4, 128.8, 126.8, 49.8, 37.4, 34.9, 29.6. HRMS (ESI^+) calcd for $C_{12}H_{15}O_3$ $[M+H]^+$ 207.1016, found 207.1017.

Procedure for Synthesis of 3-(4-nitrobenzyl)-4-oxopentanoic acid (3). Fuming nitric acid (50 mL) was added to a 100 mL round bottom flask, then placed in a low temperature reaction apparatus. 3-Benzyl-4-oxopentanoic acid (**2**) (32.5 g, 0.16 mol) was added in batches and the mixture was stirred at −15 °C for 4 h, then poured into ice water (100 mL), extracted with DCM (3 × 100 mL). The combined organic layer was washed with H_2O and brine, dried over anhydrous Na_2SO_4 and evaporated to give a yellow powder. The crude product was chromatographed on a silica gel column using petroleum ether/EtOAc/AcOH (2:1:0.03). The final product **3** was obtained as a yellow powder (28.6 g, 72.1%). mp 142.7 °C-144.1 °C. ^1H NMR (300 MHz, $CDCl_3$) δ 8.18 (d, J = 8.7 Hz, 2H), 7.34 (d, J = 8.7 Hz, 2H), 3.40–3.18 (m, 1H), 3.06 (dd, J = 13.5, 7.2 Hz, 1H), 2.78 (ddd, J = 7.41, 13.5, 8.5 Hz, 2H), 2.37 (dd, J = 17.4, 4.7 Hz, 1H), 2.14 (s, 3H). ^{13}C NMR (75 MHz, $CDCl_3$) δ 200.0, 171.6, 158.8, 124.8, 26.8, 20.5, 13.7. HRMS (ESI^+) calcd for $C_{12}H_{14}NO_5$ $[M+H]^+$ 258.0866, found 258.0866.

Procedure for the Synthesis of 5-(dibromomethylene)-4- (4-nitrobenzyl)furan-2(5*H*)-one (4) and (*Z*)-5-(bromomethylene)-4-(4-nitrobenzyl) furan-2(5*H*)-one (5). A solution of bromine (17.5 mL, 0.35 mol) in dry $CHCl_3$ (40 mL) was added slowly to an ice-cooled solution of 3-(4-nitrobenzyl)-4-oxopentanoic acid (28.6 g, 0.114 mol) in dry $CHCl_3$ (100 mL). Then the mixture was heated to reflux for 3 h then the resulting solution was washed with aqueous sodium sulfate and evaporated. The crude product was used for next step without further purification. Phosphorus pentoxide (80 g, 0.57 mol) was added with stirring to a solution of crude product in dry DCM (200 mL). The mixture was heated to reflux for 2 h, and cooled to room termperature. The resulting mixture was filtered, washed with H_2O and brine successively, dried over sodium sulfate and evaporated to produce a pale yellow oil. The crude product was chromatographed on a silica gel column using petroleum ether/EtOAc (10:1). Compound **4** was isolated as a pale solid (16.1 g, 36.3%). mp 125.3 °C-126.9 °C. ^1H NMR (300 MHz, $CDCl_3$) δ 8.26 (d, J = 8.6 Hz, 2H), 7.38 (d, J = 8.6 Hz, 2H), 5.88 (t, J = 1.6 Hz, 2H), 4.27

(d, J = 1.6 Hz, 1H). ^{13}C NMR (75 MHz, $CDCl_3$) δ 165.1, 155.3, 143.0, 130.5, 130.0, 124.5, 124.5, 122.0, 90.92, 36.1. HRMS (ESI^+) calcd for $C_{12}H_8^{79}Br_2NO_4$ $[M+1]^+$ 387.8820, found 387.8817. Compound **5** was the yellow solid (18.3 g, 51.8%). mp 116.7 °C-118.1 °C. ^{1}H NMR (300 MHz, $CDCl_3$) δ 8.21 (d, J = 8.5, 2H), 7.40 (d, J = 8.5, 2H), 6.13 (d, J = 0.5 Hz, 1H), 5.92 (d, J = 0.5 Hz, 1H), 3.94 (s, 2H). ^{13}C NMR (75 MHz, $CDCl_3$) δ 167.0, 152.3, 147.5, 142.8, 129.8, 124.4, 118.5, 90.9, 32.2. HEMS (ESI^+) calcd for $C_{12}H_9^{79}BrNO_4$ $[M+H]^+$ 309.9709, found 309.9709.

Procedure for Synthesis of 4-(4-aminobenzyl)-5- (dibromomethylene)furan-2(5*H*)-one (6). Reduced iron powder (7 g, 0.125 mol) was added to a solution of ammonium chloride (2.2 g, 0.041 mol) in H_2O (30 mL) under a nitrogen atmosphere. Then a solution of compound **5** (16.1 g, 0.041 mol) in Me_2CO (50 mL) was added dropwise and the mixture was refluxed for 4 h. Then the mixture was extracted with EtOAc. After that, the combined organic layer was basified by addition of a saturated solution of $NaHCO_3$ and the solvent was removed under reduced pressure. The crude product was chromatographed on a silica gel column using petroleum ether/EtOAc (5:1). The final product **6** was a yellow powder (11.9 g, 81.1%). mp 95.3 °C-97.1 °C.^{1}H NMR (300 MHz, $CDCl_3$) δ 6.95 (d, J = 8.4 Hz, 2H), 6.68 (d, J = 8.4 Hz, 2H), 5.82 (t, J = 1.8 Hz, 1H), 3.98 (d, J = 1.8 Hz, 2H). ^{13}C NMR (75 MHz, $CDCl_3$) δ 165.9, 159.1, 149.8, 145.8, 130.0, 125.2, 121.3, 115.7, 80.7, 36.0. HRMS (ESI^+) calcd for $C_{12}H_{10}^{81}Br_2NO_2$ $[M+H]^+$ 357.9072, found 357.9073.

Procedures for Synthesis of (*Z*)-4-(4-aminobenzyl)-5- (bromomethylene)furan-2(5*H*)-one (7). The synthesis procedure for **7** followed that of **6**. The final product was a yellow powder (14.9 g, 90.1%). mp 86.3 °C-88.1 °C. ^{1}H NMR (300 MHz, $CDCl_3$) δ 6.94 (d, J = 8.4 Hz, 2H), 6.65 (d, J = 8.4 Hz, 2H), 6.08 (s, 1H), 5.89 (s, 1H), 3.67 (s, 2H). ^{13}C NMR (75 MHz, $CDCl_3$) δ 167.7, 157.8, 152.7, 145.9, 129.7, 125.0, 117.7, 115.7, 90.3, 32.0. HRMS (ESI^+) calcd for $C_{12}H_{11}^{79}BrNO_2$ $[M+H]^+$ 279.9967, found 279.9968.

General Procedures for Synthesis of 1a-1m and 2a-2m. The acyl chloride (0.22 mmol) was added dropwise to a mixture of **6** (or **7**) (0.2 mmol) and dry pyridine (0.24 mmol) in DCM at 0 °C. The solution was stirred at room temperature overnight, then saturated NH_4Cl solution (10 mL) was added to the final mixture, then extracted with EtOAc (3 × 15 mL). Afer the combined organic phase was washed and dried, the solvent was removed. The crude product was chromatographed on a silica gel column using DCM/EtOAc (10:1).

***N*-(4-((2-(Dibromomethylene)-5-oxo-2,5-dihydrofuran-3-yl) methyl)phenyl)benamide (1a). 1a** was prepared by acylation from compound **6** and benzoyl chloride, the product was white solid (195 mg, 95%). mp 196.2 °C-198.0 °C. ^{1}H NMR (300 MHz, acetone-d_6) δ 9.58 (s, 2H), 8.03–7.96 (m, 2H), 7.88 (d, J = 8.5 Hz, 2H), 7.60–7.47 (m, 3H), 7.32 (d, J = 8.5 Hz, 2H), 6.06 (t, J = 1.6 Hz, 1H), 4.23 (d, J = 1.4 Hz, 2H). ^{13}C NMR (75 MHz, acetone-d_6) δ 166.3, 166.1, 159.0, 150.8, 139.4, 136.3, 132.4, 132.3, 130.3, 129.3, 128.3, 122.1, 121.3, 80.2, 36.0. HRMS (ESI^+) calcd for $C_{19}H_{14}^{79}Br_2NO_3$ $[M+H]^+$ 461.9340; found 461.9335.

***N*-(4-((2-(Dibromomethylene)-5-oxo-2,5-dihydrofuran-3-yl) methyl)phenyl)furan-2-carboxamide (1b). 1b** was prepared through acylation from compound **6**, the product was light yellow solid (156 mg, 90%). mp 185.3 °C-187.1 °C. ^{1}H NMR (300 MHz, DMSO-d_6) δ 10.21 (s, 1H), 7.94 (dd, J = 1.6, 0.7 Hz, 1H), 7.74 (d, J = 8.6 Hz, 2H), 7.33 (dd, J = 3.5, 0.7 Hz, 1H), 7.24 (d, J = 8.5 Hz, 2H), 6.70 (dd, J = 3.5, 1.7 Hz, 1H), 6.20 (s, 1H), 4.11 (d, J = 16.6 Hz, 2H). ^{13}C NMR (75 MHz, DMSO-d_6) δ 165.6, 157.6, 156.3, 149.3, 147.6, 145.8, 137.5, 131.4, 129.3, 121.3, 120.6, 114.8, 112.3, 81.6, 55.0, 34.4. HRMS (ESI^+) calcd for $C_{17}H_{12}^{81}Br_2NO_4$ $[M+H]^+$ 453.9108; found 453.9117.

***N*-(4-((2-(Dibromomethylene)-5-oxo-2,5-dihydrofuran-3-yl) methyl)phenyl)thiophene-2-carboxamide (1c). 1c** was prepared through acylation from compound **6** and 2-thiophenecarbonyl chloride, the product was yellow solid (250 mg, 89%). mp 199.1 °C-199.8 °C. ^{1}H NMR (300 MHz, DMSO-d_6) δ 10.25 (s, 1H), 8.02 (d, J = 3.2 Hz, 1H), 7.85 (d, J = 4.8 Hz, 1H), 7.72 (d, J = 8.4 Hz, 2H), 7.23 (dd, J = 10.0, 6.5 Hz, 3H), 6.20 (s, 1H), 4.14 (s, 2H). ^{13}C NMR (75 MHz, DMSO-d_6) δ 165.6, 160.0, 157.6, 149.3, 140.1, 137.7, 132.0, 131.4, 129.3, 129.2, 128.2, 121.3, 120.6, 81.5, 34.5. HEMS (ESI^+) calcd for $C_{17}H_{12}^{79+81}Br_2NO_3S$ $[M+H]^+$ 469.8879, found 469.8893.

***N*-(4-((2-(Dibromomethylene)-5-oxo-2,5-dihydrofuran-3-yl) methyl)phenyl)-2-phenylacetamide (1d). 1d** was prepared through acylation from compound **6** and phenylacetyl chloride, the product was white solid (200 mg, 98%). mp 188.1 °C-189.9 °C. ^{1}H NMR (300 MHz, $CDCl_3$) δ 7.44 (d, J = 8.4 Hz, 2H), 7.35 (dd, J = 13.4, 6.1 Hz, 3H), 7.06 (d, J = 8.4 Hz, 2H), 5.75 (t, J = 1.6 Hz, 1H), 4.03 (d, J = 1.1 Hz, 2H), 3.72 (s, 2H). ^{13}C NMR (75 MHz, $CDCl_3$) δ 169.4, 165.7, 157.9, 149.6, 137.2, 134.4, 131.4, 129.6, 129.3, 127.8, 121.4, 120.5, 81.0, 44.9, 36.1. HEMS (ESI^+) calcd for $C_{20}H_{16}^{79}Br_2NO_3$ $[M+H]^+$ 475.9492, found 475.9491.

***N*-(4-((2-(Dibromomethylene)-5-oxo-2,5-dihydrofuran-3-yl) methyl)phenyl)-2-(4-fluorophenyl)acetamide (1e). 1e** was prepared through acylation from compound **6** and 4-fluorophenylacetyl chloride, the product was white powder (180 mg, 90%). mp 190.6 °C-191.6 °C. ^{1}H NMR (300 MHz, DMSO-d_6) δ 10.22 (s, 1H), 7.56 (d, J = 8.5 Hz, 2H), 7.32 (dd, J = 8.5, 5.7 Hz, 2H), 7.21–7.10 (m, 4H), 6.17 (s, 1H), 4.10 (s, 2H), 3.62 (s, 2H). ^{13}C NMR (75 MHz, DMSO-d_6) δ 169.4, 163.2, 160.0, 158.1, 149.6, 138.5, 131.2, 129.7, 121.5, 119.7, 115.6, 115.3, 115.2, 81.9, 42.7, 34.8. HEMS (ESI^+) calcd for $C_{20}H_{15}^{79}Br_2FNO_3$ $[M+H]^+$ 493.9397, found 493.9397.

***N*-(4-((2-(Dibromomethylene)-5-oxo-2,5-dihydrofuran-3-yl) methyl)phenyl)-2-(4-methoxyphenyl)acetamide (1f). 1f** was prepared through acylation from compound **6** and 4-methoxyphenylacetyl chloride, the product was yellow powder (186 mg, 85%). mp 201.0 °C-202.9 °C.^{1}H NMR (300 MHz, DMSO-d_6) δ 10.15 (s, 1H), 7.58 (d, J = 8.5 Hz, 2H), 7.25 (d, J = 8.6 Hz, 2H), 7.18 (d, J = 8.5 Hz, 2H), 6.88 (d, J = 8.7 Hz, 2H), 6.14 (s, 1H), 4.09 (s, 2H), 3.72 (s, 3H), 3.55 (s, 2H). ^{13}C NMR (75 MHz, DMSO-d_6) δ 169.6, 165.6, 158.1, 157.7, 149.3, 138.3, 130.8, 130.2, 129.3, 128.0, 121.2, 119.4, 113.8, 81.5, 55.1, 42.6, 34.5. HEMS (ESI^+) calcd for $C_{21}H_{18}^{79}Br_2NO_4$ $[M+H]^+$ 505.9597, found 505.9597.

***N*-(4-((2-(Dibromomethylene)-5-oxo-2,5-dihydrofuran-3-yl) methyl)phenyl)-2-(p-tolyl)acetamide (1g). 1g** was prepared through acylation from compound **6** and 4-methylphenylacetyl chloride, the product was white solid (193 mg, 90%). mp 186.5 °C-189.1 °C. ^{1}H NMR (300 MHz, acetone-d_6) δ 9.33 (s, 2H), 7.66 (d, J = 8.5 Hz, 2H), 7.24 (t, J = 8.6 Hz, 4H), 7.12 (d, J = 7.9 Hz, 2H), 6.00 (s, 1H), 4.17 (d, J = 1.2 Hz, 2H), 3.63 (s, 2H), 2.29 (s,3H). ^{13}C NMR (75 MHz, acetone-d_6) δ 170.1, 166.1, 159.1, 150.8, 139.5, 136.9, 133.8, 131.9, 130.3, 130.0, 129.9, 122.1, 120.4, 80.2, 44.4, 36.0, 21.1. HEMS (ESI^+) calcd for $C_{21}H_{18}^{79}Br_2NO_3$ $[M+H]^+$ 489.9648, found 489.9644.

***N*-(4-((2-(Bromomethylene)-5-oxo-2,5-dihydrofuran-3-yl) methyl)phenyl)-2-(4-bromophenyl)acetamide (1h). 1h** was prepared through acylation from compound **6** and 4-bromophenylacetyl chloride, the product was yellow powder (173 mg, 91%). mp 192.5 °C-194.6 °C. ^{1}H NMR (300 MHz, DMSO-d_6) δ 10.22 (s, 1H), 7.57 (d, J = 8.5 Hz, 2H), 7.52 (d, J = 8.3 Hz, 2H), 7.29 (d, J = 8.4 Hz, 2H), 7.19 (d, J = 8.5 Hz, 2H), 6.16 (s, 1H), 4.10 (s, 2H), 3.62 (s, 2H). ^{13}C NMR (75 MHz, DMSO-d_6) δ 168.8, 165.6, 157.7, 149.0, 138.0, 135.5, 131.5, 131.3, 130.9, 129.4, 121.2, 119.9, 119.4, 42.6, 34.4. HEMS (ESI^+) calcd for $C_{20}H_{15}^{79}Br_3NO_3$ $[M+H]^+$ 553.8597, found 553.8591.

***N*-(4-((2-(Dibromomethylene)-5-oxo-2,5-dihydrofuran-3-yl) methyl)phenyl)-2-(2,6-dichlorophenyl)acetamide (1i). 1i** was prepared through acylation from compound **6** and 2,6-dichlorophenylacetyl acid, yellow powder was got (231 mg, 78%). mp 201.4 °C-202.9 °C. ^{1}H NMR (300 MHz, acetone-d_6) δ 9.51 (s, 1H), 7.67 (d, J = 6.7 Hz, 2H), 7.45 (d, J = 8.6 Hz, 2H), 7.32 (t, J = 5.9 Hz, 1H),

7.25 (d, J = 10.8 Hz, 2H), 6.04 (t, J = 1.6 Hz, 1H), 4.20 (d, J = 1.2 Hz, 2H), 4.15 (s, 2H). ^{13}C NMR (75 MHz, DMSO-d_6) δ 166.5, 165.6, 157.7, 149.2, 138.0, 135.7, 132.2, 130.9, 129.6, 129.4, 128.2, 81.6, 34.1, 13.8. HEMS (ESI$^+$) calcd for $C_{20}H_{14}^{79}Br_2^{35}Cl_2NO_3$ [M+H]$^+$ 543.8712, found 543.8708.

***N*-(4-((2-(Dibromomethylene)-5-oxo-2,5-dihydrofuran-3-yl) methyl)phenyl)-3-phenylpropanamide (1j). 1j** was prepared through acylation from compound **6** and hydrocinnamoyl chloride, the product was white solid (183 mg, 82%). mp 193.4 °C-194.9 °C. ^{1}H NMR (300 MHz, DMSO-d_6) δ 9.95 (s, 1H), 7.57 (d, J = 8.5 Hz, 2H), 7.32–7.21 (m, 4H), 7.22–7.13 (m, 3H), 6.16 (s, 1H), 4.09 (s, 2H), 2.91 (t, J = 7.6 Hz, 2H), 2.62 (t, J = 7.7 Hz, 2H). ^{13}C NMR (75 MHz, DMSO-d_6) δ 170.5, 165.6, 157.8, 149.3, 141.3, 138.2, 130.6, 129.3, 128.4, 128.4, 126.1, 121.2, 119.3, 81.5, 38.1, 34.5, 30.9. HEMS (ESI$^+$) calcd for $C_{21}H_{18}^{79}Br_2NO_3$ [M+H]$^+$ 489.9648, found 489.9451.

***N*-(4-((2-(Dibromomethylene)-5-oxo-2,5-dihydrofuran-3-yl) methyl)phenyl)cinnamamide (1k). 1k** was prepared through acylation from compound **6** and cinnamoyl chloride, the product was brown solid (250 mg, 90%). mp 193.0 °C-195.1 °C. ^{1}H NMR (300 MHz, acetone-d_6) δ 9.49 (s, 1H), 7.80 (d, J = 8.5 Hz, 2H), 7.69 (d, J = 15.6 Hz, 1H), 7.62 (dd, J = 7.6, 1.9 Hz, 2H), 7.46–7.36 (m, 2H), 7.29 (d, J = 8.5 Hz, 2H), 6.87 (d, J = 15.6 Hz, 1H), 6.04 (t, J = 1.6 Hz, 1H), 4.21 (d, J = 1.3 Hz, 2H). ^{13}C NMR (75 MHz, acetone-d_6) δ 166.2, 164.6, 159.1, 150.8, 141.8, 139.6, 136.1, 132.2, 130.6, 130.4, 129.9, 128.7, 123.0, 122.2, 120.6, 80.3, 36.1. HEMS (ESI$^+$) calcd for $C_{21}H_{16}^{79+81}Br_2NO_3$ [M+H]$^+$ 487.9491, found 487.9494.

***N*-(4-((2-(Dibromomethylene)-5-oxo-2,5-dihydrofuran-3-yl) methyl)phenyl)-3-(4-methoxyphenyl)acrylamide (1l). 1l** was prepared through acylation from compound **6** and 4-methoxycinnamic acid, the product was white solid (125 mg, 70%). mp 188.6 °C-190.4 °C. ^{1}H NMR (300 MHz, DMSO-d_6) δ 10.16 (s, 1H), 7.69 (d, J = 8.6 Hz, 2H), 7.60–7.51 (m, 4H), 7.21 (d, J = 8.6 Hz, 2H), 7.00 (d, J = 8.8 Hz, 2H), 6.69 (d, J = 15.5 Hz, 1H), 6.20 (s, 1H), 4.13 (s, 2H), 3.80 (s, 3H). ^{13}C NMR (75 MHz, DMSO-d_6) δ 166.0, 164.3, 161.1, 158.1, 149.6, 140.4, 138.7, 131.2, 129.8, 129.8, 127.7, 120.1, 119.7, 119.8, 114.9, 81.9, 55.8, 34.8. HRMS (ESI$^+$) calcd for $C_{22}H_{18}^{81}Br_2NO_4$ [M+H]$^+$ 519.9578, found 519.9588.

***N*-(4-((2-(Dibromomethylene)-5-oxo-2,5-dihydrofuran-3-yl) methyl)phenyl)-2-(3,4,5-trimethoxyphenyl)acetamide (1m). 1m** was prepared through acylation from compound **6** and 3,4,5-trimethoxyphenylacetic chloride, the product was white powder (212 mg, 92%). mp 195.6 °C-199.3 °C. ^{1}H NMR (300 MHz, acetone-d_6) δ 9.96 (s, 1H), 7.89 (d, J = 8.6 Hz, 2H), 7.62 (s, 2H), 7.38 (d, J = 8.6 Hz, 2H), 6.08 (t, J = 1.6 Hz, 1H), 4.27 (d, J = 1.3 Hz, 2H), 3.90 (s, 6H), 3.86 (s, 3H). ^{13}C NMR (75 MHz, DMSO-d_6) δ 175.6, 171.3, 169.1, 166.0, 158.0, 149.6, 138.4, 135.8, 131.9, 131.6, 131.3, 129.7, 121.6, 120.2, 119.8, 81.9, 42.9. HEMS (ESI$^+$) calcd for $C_{23}H_{22}^{79}Br_2NO_6$ [M+H]$^+$ 565.9808, found 565.9806.

(*Z*)-*N*-(4-((2-(Bromomethylene)-5-oxo-2,5-dihydrofuran-3-yl)methyl)phenyl)benzamide (2a). 2a was prepared through acylation from compound **7** and benzoyl chloride, the product was white solid (230 mg, 90%). mp 185.1 °C-186.6 °C. ^{1}H NMR (300 MHz, DMSO-d_6) δ 10.28 (s, 1H), 7.95 (d, J = 7.1 Hz, 2H), 7.76 (d, J = 8.1 Hz, 2H), 7.55 (dt, J = 14.2, 7.0 Hz, 3H), 7.31 (d, J = 8.1 Hz, 2H), 6.91 (s, 1H), 6.27 (s, 1H), 3.89 (s, 2H). ^{13}C NMR (75 MHz, DMSO-d_6) δ 167.6, 165.6, 158.2, 152.0, 138.2, 135.0, 131.9, 131.7, 129.2, 128.5, 127.8, 120.7, 117.0, 92.1, 30.9. HEMS (ESI$^+$) calcd for $C_{19}H_{15}^{79}BrNO_3$ [M+H]$^+$ 384.0230, found 384.0229.

(*Z*)-*N*-(4-((2-(Bromomethylene)-5-oxo-2,5-dihydrofuran-3-yl)methyl)phenyl)furan-2-carboxamide (2b). 2b was prepared through acylation from compound **7** and 2-furoyl chloride, he product was yellow solid (159 mg, 84%). mp 183.9 °C-186.1 °C. ^{1}H NMR (300 MHz, acetone-d_6) δ 9.46 (s, 1H), 7.84 (d, J = 8.5 Hz, 2H), 7.75 (s, 1H), 7.33 (d, J = 8.5 Hz, 2H), 7.21 (d, J = 3.5 Hz, 1H), 6.68–6.59 (m, 2H), 6.13 (s, 1H), 3.97 (s, 2H). ^{13}C NMR (75 MHz, acetone-d_6) δ 168.0, 158.8, 157.0, 153.6, 149.1, 145.9, 138.7, 132.8, 130.1, 121.3, 118.2, 115.4, 113.1, 90.9, 32.1. HEMS (ESI$^+$) calcd for $C_{17}H_{13}^{79}BrNO_4$ [M+H]$^+$ 374.0023, found 374.0023.

(*Z*)-*N*-(4-((2-(Bromomethylene)-5-oxo-2,5-dihydrofuran-3-yl)methyl)phenyl)thiophene-2-carboxamide (2c). 2c was prepared through acylation from compound **7** and 2-thiophenecarbonyl chloride, he product was yellow solid (159 mg, 84%). mp 188.1 °C-189.1 °C. ^{1}H NMR (300 MHz, acetone-d_6) δ 9.57 (s, 1H), 7.89 (d, J = 3.1 Hz, 1H), 7.77 (dd, J = 6.6, 4.6 Hz, 3H), 7.32 (d, J = 8.4 Hz, 2H), 7.22–7.11 (m, 1H), 6.64 (s, 1H), 6.12 (s, 1H), 3.97 (s, 2H). ^{13}C NMR (75 MHz, acetone-d_6) δ 168.0, 160.8, 158.8, 153.6, 141.4, 139.0, 132.7, 132.2, 130.1, 129.2, 128.7, 121.3, 118.2, 90.9, 32.1. HEMS (ESI$^+$) calcd for $C_{17}H_{13}^{79}BrNO_3S$ [M+H]$^+$ 389.9834, found 389.9830.

(*Z*)-*N*-(4-((2-(Bromomethylene)-5-oxo-2,5-dihydrofuran-3-yl)methyl)phenyl)-2-phenylacetamide (2d). 2d was prepared through acylation from compound **7** and phenylacetyl chloride, and the yield was 98%, white solid 187 mg mp 188.6 °C-190.4 °C. ^{1}H NMR (300 MHz, acetone-d_6) δ 9.39 (s, 1H), 7.64 (d, J = 8.5 Hz, 2H), 7.36 (t, J = 7.9 Hz, 2H), 7.34–7.27 (m, 2H), 7.24 (dd, J = 9.1, 2.4 Hz, 3H), 6.60 (s, 1H), 6.07 (s, 1H), 3.90 (s, 2H), 3.69 (s, 2H). ^{13}C NMR (75 MHz, acetone-d_6) δ 169.8, 167.9, 158.7, 153.4, 139.3, 136.7, 132.2, 130.0, 129.9, 129.1, 127.4, 120.4, 118.0, 90.8, 44.6, 32.0. HEMS (ESI$^+$) calcd for $C_{20}H_{17}^{79}BrNO_3$ [M+H]$^+$ 398.0386, found 398.0400.

(*Z*)-*N*-(4-((2-(Bromomethylene)-5-oxo-2,5-dihydrofuran-3-yl)methyl)phenyl)-2-(4-fluorophenyl)acetamide (2e). 2e was prepared through acylation from compound **7** and 4-fluorophenylacetyl chloride, the product was white solid (241 mg, 88%). mp 188.1 °C-189.6 °C. ^{1}H NMR (300 MHz, acetone-d_6) δ 9.41 (s, 1H), 7.64 (d, J = 8.6 Hz, 2H), 7.40 (dd, J = 8.7, 5.5 Hz, 2H), 7.25 (d, J = 8.6 Hz, 2H), 7.06 (dd, J = 12.3, 5.5 Hz, 2H), 6.60 (s, 1H), 6.08 (s, 1H), 3.92 (s, 2H), 3.63 (s, 2H). ^{13}C NMR (75 MHz, acetone-d_6) δ 169.7, 167.9, 164.2, 160.9, 158.7, 153.4, 139.2, 132.8, 132.7, 132.2, 132.1, 131.9, 131.8, 131.7, 130.0, 120.4, 118.0, 115.8, 115.7, 115.6, 115.5, 90.8, 43.5, 32.0. HEMS (ESI$^+$) calcd for $C_{20}H_{16}^{79}BrFNO_3$ [M+H]$^+$ 416.0292, found 416.0295.

(*Z*)-*N*-(4-((2-(Bromomethylene)-5-oxo-2,5-dihydrofuran-3-yl)methyl)phenyl)-2-(4-methoxyphenyl)acetamide (2f). 2f was prepared through acylation from compound **7** and 4-methoxyphenylacetyl chloride, the product was light yellow solid (253 mg, 89%). mp 175.8 °C-178.1 °C. ^{1}H NMR (300 MHz, acetone-d_6) δ 9.34 (s, 1H), 7.63 (d, J = 8.5 Hz, 2H), 7.28 (d, J = 8.6 Hz, 2H), 7.24 (d, J = 8.5 Hz, 2H), 6.86 (d, J = 8.7 Hz, 2H), 6.59 (s, 1H), 6.06 (s, 1H), 3.90 (s, 2H), 3.75 (s, 3H), 3.61 (s, 2H). ^{13}C NMR (75 MHz, acetone-d_6) δ 170.2, 167.9, 159.4, 158.7, 153.3, 139.2, 132.0, 130.9, 129.9, 128.5, 120.3, 117.9, 114.5, 90.8, 55.3, 43.7, 31.9. HEMS (ESI$^+$) calcd for $C_{21}H_{19}^{79}BrNO_4$ [M+H]$^+$ 428.0492, found 428.0291.

(*Z*)-*N*-(4-((2-(Bromomethylene)-5-oxo-2,5-dihydrofuran-3-yl)methyl)phenyl)-2-(*p*-tolyl)acetamide (2g). 2g was prepared through acylation from compound **7** and 4-methylphenylacetyl chloride, the product was light brown solid (168 mg, 79%). mp 171.4 °C-173.1 °C. ^{1}H NMR (300 MHz, acetone-d_6) δ 9.33 (s, 1H), 7.63 (d, J = 8.5 Hz, 2H), 7.25 (d, J = 8.2 Hz, 4H), 7.12 (d, J = 7.9 Hz, 2H), 6.61 (s, 1H), 6.08 (s, 1H), 3.91 (s, 2H), 3.63 (s, 2H), 2.28 (s, 3H). ^{13}C NMR (75 MHz, acetone-d_6) δ 170.1, 168.1, 158.9, 153.6, 139.5, 136.9, 133.8, 132.2, 130.1, 130.0, 129.9, 129.8, 120.5, 118.1, 90.9, 44.4, 32.1, 21.1. HEMS (ESI$^+$) calcd for $C_{21}H_{19}^{79}BrNO_3$ [M+H]$^+$ 412.0498, found 412.0498.

(*Z*)-*N*-(4-((2-(Bromomethylene)-5-oxo-2,5-dihydrofuran-3-yl)methyl)phenyl)-2-(4-bromophenyl)acetamide (2h). 2h was prepared through acylation from compound **7** and 4-bromophenylacetic acid, the product was yellow solid (241 mg, 78%). mp 183.5 °C-185.1 °C. ^{1}H NMR (300 MHz, DMSO-d_6) δ 10.20 (s, 1H), 7.55 (d, J = 8.5 Hz, 2H), 7.50 (d, J = 8.4 Hz, 2H), 7.33 (d, J = 8.4 Hz, 2H), 7.26 (d, J = 8.5 Hz, 2H), 6.96 (s, 1H), 6.24 (s, 1H), 3.85

(s, 2H), 3.62 (s, 2H). ^{13}C NMR (75 MHz, DMSO-d_6) δ 169.1, 167.9, 158.5, 152.4, 138.4, 135.8, 131.9, 131.6, 129.6, 120.2, 119.8, 117.3, 92.4, 43.9, 31.2. HEMS (ESI$^+$) calcd for $C_{20}H_{16}^{79}Br_2NO_3$ [M+H]$^+$ 477.9472, found 477.9471.

(*Z*)-*N*-(4-((2-(Bromomethylene)-5-oxo-2,5-dihydrofuran-3-yl)methyl)phenyl)-2-(2,6-dichlorophenyl)acetamide (2i). 2i was prepared through acylation from compound **7** and 2,6-dichlorophenylacetic acid, the product was white solid (120 mg, 75%). mp 182.6 °C-184.9 °C. ^{1}H NMR (300 MHz, DMSO-d_6) δ 10.33 (s, 1H), 7.54 (d, J = 8.4 Hz, 2H), 7.48 (d, J = 8.0 Hz, 2H), 7.36–7.30 (t, 1H), 7.25 (d, J = 8.4 Hz, 2H), 6.95 (s, 1H), 6.24 (s, 1H), 4.04 (s, 2H), 3.85 (s, 2H). ^{13}C NMR (75 MHz, DMSO-d_6) δ 167.5, 166.5, 158.1, 151.9, 138.0, 135.6, 132.2, 131.4, 129.5, 129.2, 128.2, 119.3, 116.9, 92.0, 38.5, 30.7. HEMS (ESI$^+$) calcd for $C_{20}H_{15}^{81}Br^{37}Cl_2NO_3$ [M+H]$^+$ 467.9584, found 467.9561.

(*Z*)-*N*-(4-((2-(Bromomethylene)-5-oxo-2,5-dihydrofuran-3-yl)methyl)phenyl)-3-phenylpropanamide (2j). 2j was prepared through the acylation from compound **7** and hydrocinnamoyl chloride, the product was yellow solid (198 mg, 95%). mp 178.4 °C-179.9 °C. ^{1}H NMR (300 MHz, acetone-d_6) δ 9.20 (s, 1H), 7.64 (d, J = 8.5 Hz, 2H), 7.22–7.33 (m, 6H), 7.16 (d, J = 8.5 Hz, 2H), 6.62 (s, 1H), 6.09 (s, 1H), 3.92 (s, 2H), 2.99 (t, J = 7.7 Hz, 2H), 2.68 (t, J = 7.7 Hz, 2H). ^{13}C NMR (75 MHz, acetone-d_6) δ 170.7, 167.6, 158.4, 153.1, 141.9, 139.0, 131.6, 129.6, 128.8, 126.4, 119.9, 117.6, 90.4, 38.9, 31.7, 31.6. HEMS (ESI$^+$) calcd for $C_{21}H_{19}^{79}BrNO_3$ [M+H]$^+$ 412.0575, found 412.0571.

(*Z*)-*N*-(4-((-2-(Bromomethylene)-5-oxo-2,5-dihydrofuran-3-yl)methyl)phenyl)cinnamamide (2k). 2k was prepared through the acylation from compound **7** and cinnamoyl chloride, the product was white solid (253 mg, 94%). mp 184.6 °C-186.3 °C. ^{1}H NMR (300 MHz, acetone-d_6) δ 9.44 (s, 1H), 7.77 (d, J = 8.5 Hz, 2H), 7.69 (d, J = 15.6 Hz, 1H), 7.62 (dd, J = 7.5, 1.9 Hz, 2H), 7.49–7.36 (m, 4H), 7.31 (d, J = 8.5 Hz, 3H), 6.85 (d, J = 15.6 Hz, 1H), 6.65 (s, 1H), 6.12 (s, 1H), 3.96 (s, 2H). ^{13}C NMR (75 MHz, acetone-d_6) δ 167.7, 164.1, 158.5, 153.3, 141.4, 139.2, 135.7, 132.1, 130.3, 129.9, 129.5, 128.3, 122.5, 120.2, 117.8, 90.5, 31.8. HEMS (ESI$^+$) calcd for $C_{21}H_{17}^{79}BrNO_3$ [M+H]$^+$ 410.0386, found 410.0385.

(*Z*)-*N*-(4-((-2-(Bromomethylene)-5-oxo-2,5-dihydrofuran-3-yl)methyl)phenyl)-3- (4-methoxyphenyl)acrylamide (2l). 2l was prepared through the acylation reaction of compound **7** and 4-methoxycinnamic acid, the product was white solid (132 mg, 78%). mp 185.4 °C-187.3 °C. ^{1}H NMR (300 MHz, acetone-d_6) δ 9.37 (s, 1H), 7.77 (d, J = 8.5 Hz, 2H), 7.64 (d, J = 15.6 Hz, 1H), 7.55 (d, J = 8.7 Hz, 2H), 7.55 (d, J = 8.7 Hz, 2H), 7.29 (d, J = 8.5 Hz, 2H), 6.96 (d, J = 8.8 Hz, 2H), 6.71 (d, J = 15.6 Hz, 1H), 6.64 (s, 1H), 6.11 (s, 1H), 3.95 (s, 2H), 3.83 (s, 3H). ^{13}C NMR (75 MHz, acetone-d_6) δ 168.1, 164.9, 162.1, 158.9, 153.6, 141.5, 139.7, 132.2, 130.3, 130.2, 128.6, 120.6, 120.3, 118.2, 115.2, 90.9, 55.8, 32.2. HEMS (ESI$^+$) calcd for $C_{22}H_{19}^{79}BrNO_4$ [M+H]$^+$ 440.0492, found 440.0486.

(*Z*)-*N*-(4-((2-(Bromomethylene)-5-oxo-2,5-dihydrofuran-3-yl)methyl)phenyl)-2-(3,4,5-trimethoxyphenyl)acetamide (2m). 2m was prepared through acylation from compound **7** and 3,4,5-trimethoxyphenylacetic chloride, the product was white solid (230 mg, 94%). mp 190.1 °C-191.3 °C. 1H NMR (300 MHz, DMSO-d_6) δ 10.11 (s, 1H), 7.56 (d, J = 8.5 Hz, 2H), 7.16 (d, J = 8.4 Hz, 2H), 6.63 (s, 2H), 6.13 (s, 1H), 4.07 (s, 2H), 3.74 (s, 6H), 3.61 (s, 3H), 3.53 (s, 2H). ^{13}C NMR (75 MHz, DMSO-d_6) δ 169.5, 166.0, 158.1, 153.1, 149.6, 138.5, 136.7, 131.9, 131.2, 129.7, 121.5, 119.8, 106.9, 81.8, 60.4, 56.3, 44.0, 34.8. HEMS (ESI$^+$) calcd for $C_{23}H_{23}^{79}BrNO_6$ [M+H]$^+$ 488.0703, found 488.0714.

Bacterial Culture. In this work, *P. aeruginosa* reporter strain PAO1-lasB-gfp strain PAO1-rhlA-gfp strain and PAO1-pqsA-gfp strain, which was kindly provided by Singapore Centre for Environmental Life Sciences Engineering, stored at −80 °C was used to study the effects of new compounds by QS Inhibition Assays. A single colony was cultured in Luria-Bertani (LB) broth with 300 μg/mL carbenicillin and 60 μg/mL gentamicin for 18 h at 37 °C.

***P. aeruginosa* QS Inhibition Assays.** To assess the impact of the compounds on QS signaling, the *P. aeruginosa* reporter strain PAO1-*lasB-gfp* strain PAO1-rhlA-gfp strain and PAO1-*pqsA-gfp* strain, which harbors a fusion of the *lasB* promoter or *rhlA* promoter or *pqsA* promoter to an unstable *gfp*(ASV) gene and responds to the signalling molecules respectly, was used. The test compounds were dissolved in DMSO to 10 mM for storage and diluted in LB medium to a final concertration of 10 μM for assay. Furanone C-30 was selected as positive control. Bacteria were cultured in Luria-Bertani broth (LB) at 37 °C with shaking at 200 rpm for 18 h and then an inoculating culture was prepared by diluting the overnight culture 1:100 into fresh LB medium. Finally 100 μL of bacterial suspension and 100 μL diluted compounds were added to the wells. DMSO control (0.1% final concentration) and blank control were used. The *gfp*(ASV) expression (fluorescence, excitation 485 nm, emission 528 nm) was measured every 15 min at 37 °C by the use of a microplate reader (Bio-Rad Laboratories, CA, USA) for at least 12 h. The inhibition assay for all test compounds and controls were done in triplicate manner [55].

Growth measurement. The steps to measure the growth of *P. aeruginosa* was similar to QS inhibition assays. The overnight cultured *P. aeruginosa* strain PAO1 was diluted with fresh LB medium and the compounds were also diluted to appropriate concentration. Bacterial suspension and diluted compounds were equally added to the 96-well plates. Last the growth curve was evaluated every 15 min at 37 °C by measuring OD_{600} using a microplate reader (Bio-Rad Laboratories, CA, USA) for at least 12 h.

Cell Culture. The murine RAW264.7 macrophage cells were obtained from the American Type Culture Collection (ATCC) and cultured in Dulbecco's modified Eagle's medium (DMEM) supplemented with 10% fetal bovine serum, penicillin (100 units/mL) and streptomycin (100 μg/mL) at 37 °C in a 5% CO_2 humidified atmosphere.

Assay for NO Production. Nitrite level, an index for NO production, was measured in the supernatant of RAW264.7 cells by the Griess methol [56]. RAW 264.7 cells were inoculated to 96-well plates at the density of 5 × 10^4 cells per well and cultured for 18 h. Different compounds at the concentration of 10 μM were added to each well and then was additionally treated the LPS (100 ng/mL) and incubated at 37 °C for 48 h. After stimulated for 48 h by LPS, the supernatant of the cell culture medium and the same volume of Griess reagent (1% sulfanilamide and 0.1% N-(1-naphthyl)ethylenediamine dihydrochloride in 5% phosphoric acid) were added to a 96-well plate for 10 min, and nitrite was measured at 540 nm (OD_{540}) using a microplate reader (Bio-Rad Laboratories, CA, USA). Meanwhile, the results were evaluated from three independent experiments.

NO inhibition rate (%) = [control (OD_{540}) - compound (OD_{540})]/[control (OD_{540}) - blank (OD_{540})] × 100.

Control: the cells treated with LPS only.

Compound: the cells treated with LPS and compounds.

Blank: the cells cultured with fresh medium only.

Cell Cytotoxicity. Cell cytotoxicity was assessed by the 3-[4,5-dimethylthiazol-2-yl]-2,5- diphenyltetrasolium bromide (MTT) assay. In brief, RAW264.7 cells (4 × 10^3 cells/well) were seeded in 96-well plate containing DMEM supplemented with 10% FBS and treated with different compounds which were diluted in DMEM for 48 h. After treatment, 20 μL of 0.5 mg/mL MTT reagent was added and incubated with in the dark for 4 h. Then, the medium was removed and 150 μL DMSO was added to dissolve formazone crystals for measurement at 570 nm (OD_{570}) with a microplate reader. Cell viability was given as relative value to the control in percent from three independent experiments.

Cell viability (%) = compound (OD_{570})/control (OD_{570}) × 100.

Control: the cells cultured with fresh medium only.

Compound: the cells treated with compounds or LPS.

Measurement of TNF-α and IL-6. Production of the pro-inflammatory cytokines was evaluated by an enzyme-linked immunosorbent assay (ELISA). RAW264.7 cells (5×10^5 cells/well) were pretreated with or without 10 μM of compounds in 24-well plates for 2 h, and then the cells were stimulated with 100 ng/mL LPS and cultured for 6 h, 12 h and 24 h to assay TNF-α and IL-6 production. The levels of TNF-α and IL-6 were measured using a specific ELISA kit (TNF-α: MultiSciences, EK2822; IL-6: MultiSciences, EK2062) according to the manufacturer's instructions, and were read at 450 nm (OD_{450}) in a microplate reader. LPS was used as the positive control in parallel experiments. The results were calculated from three independent experiments.

Western Blot Analysis. RAW264.7 cells (2×10^6 cells/well) were pretreated with or without compounds for 1 h in 6-well plates. After treatment, cells were stimulated with LPS (500 ng/mL) for 4 h. The cells were collected and washed with ice-cold phosphate buffered saline (PBS), and the extract proteins were lysed with IP buffer (Beyotime, P0013) containing with 1 mM phenylmethanesulfonyl fluoride (PMSF: Beyotime, ST506) for 30 min at 4 °C. Then cell lysates were centrifuged at 4 °C to collect the supernatant. Total protein concentration was quantitated with the BCA protein assay kit (Thermo Scientific, 23227). The samples (20 μg of protein) were mixed with loading buffer, separated on 12.5% SDS polyacrylamide gels, and transferred onto polyvinylidene fluoride (PVDF) membranes (Millipore, USA). The PVDF membranes were blocked at room temperature with 5% non-fat dry milk in Tris-buffered saline Tween-20 (TBST) buffer and then were incubated while shaking with targeted primary antibodies, including anti-phosphorylation of ERK1/2 (Thr202/Tyr204), anti-ERK1/2, anti-phosphorylation of p38 (Thr180/Tyr182), anti-p38, anti-phosphorylation of IκBα (Ser32/36), anti-IκBα, anti-phosphorylation of NF-κB p65, anti-NF-κB p65, and β-actin, overnight at 4 °C overnight. All the primary antibodies were purchased from Cell Signaling Technology. Then, the PVDF membrane was washed three times with TBST buffer and incubated with anti-rabbit or anti-mouse HRP-conjugated secondary antibody for 90 min at room temperature. Finally, the membranes were washed with TBST and exposed to ECL reagents. Protein level was normalized to the matching densitometric value of the internal control.

Molecular Modeling. In present work, we employed the structure of PPARγ (PDB ID: 2PRG) to complete this docking experiment. First, the structures of **2e**, **2k**, rosiglitazone and indomethacin were built by the sketching program in SYBYL 8.1 molecular modeling package of Tripos, and the minimized energy structures of these four ligands were performed by using the Tripos molecular mechanics force field. Second, all ligands were removed and the polar hydrogen atoms were added. Other parameters were established by defaults in the software. Third, the docking calculation was performed using the empirical scoring function in Surflex-Dock. The Molecular Computer Aided Design (MOLCAD) program was also developed and displayed with cavity depth potential and hydrogen bond site to further explore the interaction between these four compounds and the PPARγ receptor.

Animals. Male SPF mice (body weight of 20 ± 2 g) were acquired from the Guangdong Medical Laboratory Animal Center (Guangzhou, China). Animals were housed in a 23 ± 2 °C temperature with a 12/12 h light-dark cycle and fed with standard rodent diet which was also provided by Guangdong Medical Laboratory Animal Center and water. The mice were acclimatized to the laboratory for at least 7 days before use. All experimental protocols involving the experiment were in accordance with the guidelines set out by the Institutional Animal Care and Use Committee of China Pharmaceutical University.

LPS-Induced Inflammatory Mortality in SPF Mice. Compounds were dissolved in DMSO, then stroke-physiological saline solution was added to the concentration of 20 mg/kg. Male SPF mice were randomly divided into five groups (n = 10 mice/group) and i.v. injection with high dose (20 mg/kg), low dose (5 mg/kg) of **2e**, or 20 mg/kg of rosiglitazone. 6 days later, LPS was i.v. injected (20 mg/kg). Control group received a similar volume of vehicle. Then, the mortality was recorded for 7 days.

Statistical Analysis. All data in the text were presented as the arithmetic mean ± standard deviation (SD) of at least three independent experiments, and values of $p < 0.05$ and $p < 0.01$ were considered to be statistically significant.

Acknowledgment

This work was supported by the National Natural Science Foundation of China (81072554, 81673336) and the Fundamental Research Funds for the Central University (No. 21617478).

Appendix A. Supplementary data

Supplementary data related to this article can be found at https://doi.org/10.1016/j.ejmech.2017.11.085.

Abbreviations used

QS, quorum-sensing; NF-κB, nuclear factor-kappa B; MAPK, mitogen-activated protein kinase; PPARγ, peroxisome proliferator-activated receptor γ; LPS, lipopolysaccharides; $3OC_{12}$-HSL, 3-oxododecanoyl homoserine lactone; TNF-α, tumor necrosis factor α; PPARγ, Peroxisome proliferator-activated receptor gamma; IL-6, interleukin-6; AHL, N-acyl homoserine lactones; NMR, nuclear magnetic resonance; MS, mass spectrometry; HRMS, high resolution mass spectrometry; NO, nitric oxide; MTT, 3-(4,5-dimethylthiazol-2-yl)-2,5-diphenyltetrazolium bromide; ELISA, enzyme linked immunosorbent assay; IκB-α, inhibitor kappa B alpha; ERK, extracellular regulated protein kinases; DCM, dichloromethane; DMSO, dimethyl sulfoxide; LB, Luria-Bertani; DMEM, Dulbecco's modified Eagle's medium; PBS, phosphate buffered saline; PMSF, phenylmethanesulfonyl fluoride; PVDF, polyvinylidene fluoride; TBST, Tris-buffered saline Tween-20; MOLCAD, Molecular Computer Aided Design.

References

[1] K. Beckrich, S.A. Aronovitch, Hospital-acquired pressure ulcers: a comparison of costs in medical vs. surgical patients, Nurs. Econ. 17 (1999) 263–271.
[2] E.J. Boyko, J.H. Ahroni, D.G. Smith, D. Davignon, Increased mortality associated with diabetic foot ulcers, Diabet. Med. 13 (1996) 967–972.
[3] B.M. Peters, M.A. Jabra-Rizk, A.O. Graeme, J.W. Costerton, M.E. Shirtliff, Polymicrobial interactions: impact on pathogenesis and human disease, Clin. Microbiol. Rev. 25 (2012) 193–213.
[4] K. Papenfort, B.L. Bassler, Quorum sensing signal-response systems in Gram-negative bacteria, Nat. Rev. Microbiol. 14 (2016) 576–588.
[5] J. Cohen, The immunopathogenesis of sepsis, Nature 420 (2002) 885–891.
[6] S. Cuzzocrea, B. Pisano, L. Dugo, A. Ianaro, P. Maffia, N.S. Patel, R. Di Paola, A. Ialenti, T. Genovese, P.K. Chatterjee, F. Fulia, E. Cuzzocrea, M. Di Rosa, A.P. Caputi, C. Thiemermann, Rosiglitazone, a ligand of the peroxisome proliferator-activated receptor-gamma, reduces acute inflammation, Eur. J. Pharmacol. 834 (2004) 79–93.
[7] J. Overhage, A. Campisano, M. Bains, E.C. Torfs, B.H. Rehm, R.E. Hancock, Human host defense peptide LL-37 prevents bacterial biofilm formation, Infect. Immun. 76 (2008) 4176–4182.
[8] R. Ramos, J.P. Silva, A.C. Rodrigues, R. Costa, L. Guardão, F. Schmitt, R. Soares, M. Vilanova, L. Domingues, M. Gama, Wound healing activity of the human antimicrobial peptide LL37, Peptides 32 (2011) 1469–1476.
[9] A. Grönberg, M. Mahlapuu, M. Ståhle, C. Whately-Smith, O. Rollman, Treatment with LL-37 is safe and effective in enhancing healing of hard-to-heal venous leg ulcers: a randomized, placebo-controlled clinical trial, Wound

Repair Regen. 22 (2014) 613–621.
[10] A. Henriques, S. Jackson, R. Cooper, N. Burton, Free radical production and quenching in honeys with wound healing potential, J. Antimicrob. Chem. 58 (2006) 773–777.
[11] G.T. Gethin, S. Cowman, R.M. Conroy, The impact of Manuka honey dressings on the surface pH of chronic wounds, Int. Wound J. 5 (2008) 185–194.
[12] A. Seckam, R. Cooper, Understanding how honey impacts on wounds: an update on recent research findings, Int. Wound J. 4 (2013) 20–24.
[13] M. Subrahmanyam, Honey impregnated gauze versus polyurethane film (OpSite) in the treatment of burns-a prospective randomised study, Br. J. Plast. Surg. 46 (1993) 322–323.
[14] A. Asher, T.A. Mashhood, Khan, A.N. Sami, Honey compared with 1% silver sulfadiazine cream in the treatment of superficial and partial thickness burns, J. Pak. Assoc. Dermatol 16 (2006) 14–19.
[15] Y. Wan, R.M. Evans, Rosiglitazone activation of PPARgamma suppresses fractalkine signaling, J. Mol. Endocrinol. 44 (2010) 135–142.
[16] K. Wada, Y. Kamisaki, Anti-inflammatory effect of PPARgamma agonists: basics and clinical applications, Nihon Rinsho 68 (2010) 278–283.
[17] K. Celinski, T. Dworzanski, R. Fornal, A. Korolczuk, A. Madro, T. Brzozowski, M. Slomka, Comparison of anti-inflammatory properties of peroxisome proliferator-activated receptor gamma agonists rosiglitazone and troglitazone in prophylactic treatment of experimental colitis, J. Physiol. Pharmacol. 64 (2013) 587–595.
[18] S. Cuzzocrea, B. Pisano, L. Dugo, A. Ianaro, P. Maffia, N.S. Patel, R. Di Paola, A. Ialenti, T. Genovese, P.K. Chatterjee, F. Fulia, E. Cuzzocrea, M. Di Rosa, A.P. Caputi, C. Thiemermann, Rosiglitazone, a ligand of the peroxisome proliferator-activated receptor-gamma, reduces acute inflammation, Eur. J. Pharmacol. 483 (2004) 79–93.
[19] A. Jahoor, R. Patel, A. Bryan, C. Do, J. Krier, C. Watters, W. Wahli, G. Li, S.C. Williams, K.P. Rumbaugh, Peroxisome proliferator-activated receptors mediate host cell proinflammatory responses to Pseudomonas aeruginosa autoinducer, J. Bacteriol. 190 (2008) 4408–4415.
[20] M. Hentzer, K. Riedel, T.B. Rasmussen, A. Heydorn, J.B. Andersen, M.R. Parsek, S.A. Rice, L. Eberl, S. Molin, N. Høiby, S. Kjelleberg, Inhibition of quorum sensing in Pseudomonas aeruginosa biofilm bacteria by a halogenated furanone compound, Microbiology 148 (2002) 87–102.
[21] J.L. Guo, B.Z. Li, W.M. Chen, P.H. Sun, Y. Wang, Synthesis of substituted 1H-pyrrol-2 (5*H*)-ones and 2 (5*H*)-furanones as inhibitors of P. aeruginosa biofilm, Lett. Drug Des. Discov. 6 (2009) 107–113.
[22] G.Y. Liu, B.Q. Guo, W.N. Chen, C. Cheng, Q.L. Zhang, M.B. Dai, J.R. Sun, P.H. Sun, W.M. Chen, Synthesis, molecular docking, and biofilm formation inhibitory activity of 5-substituted 3, 4-Dihalo-5*H*-furan-2-one derivatives on Pseudomonas aeruginosa, Chem. Biol. Drug Des. 79 (2012) 628–638.
[23] P.H. Sun, Z.Q. Yang, M.K. Li, W.M. Chen, Q. Liu, X.S. Yao, 3D-QSAR study of synthetic furanones as inhibitors of quorum sensing by using CoMFA and CoMSIA approach, Lett. Drug Des. Discov. 6 (2009) 568–574.
[24] Y.S. Tung, M.S. Coumar, Y.S. Wu, H.Y. Shiao, J.Y. Chang, J.P. Liou, P. Shukla, C.W. Chang, C.Y. Chang, C.C. Kuo, T.K. Yeh, Scaffold-hopping strategy: synthesis and biological evaluation of 5, 6-fused bicyclic heteroaromatics to identify orally bioavailable anticancer agents, J. Med. Chem. 54 (2011) 3076–3080.
[25] Q. Chen, W. Tian, G. Han, J. Qi, C. Zheng, Y. Zhou, L. Ding, J. Zhao, J. Zhu, J. Lv, C. Sheng, Design and synthesis of novel benzoheterocyclic derivatives as human acrosin inhibitors by scaffold hopping, Eur. J. Med. Chem. 59 (2013) 176–182.
[26] K.S. Smalley, W. Feniuk, L.A. Sellers, P.P. Humphrey, The pivotal role of phosphoinositide-3 kinase in the human somatostatin sst 4 receptor-mediated stimulation of p44/p42 mitogen-activated protein kinase and extracellular acidification, Biochem. Biophys. Res. Commun. 263 (1999) 239–243.
[27] M.A. Brogley, M. Cruz, H.S. Cheung, Basic calcium phosphate crystal induction of collagenase 1 and stromelysin expression is dependent on a p42/44 mitogen-activated protein kinase signal transduction pathway, J. Cell. Physiol. 180 (1999) 215–224.
[28] Y.H. Wang, R.A. Maurer, A role for the mitogen-activated protein kinase in mediating the ability of thyrotropin-releasing hormone to stimulate the prolactin promoter, Mol. Endocrinol. 13 (1999) 1094–1104.
[29] S.M. Park, H.S. Kim, J. Choe, T.H. Lee, Differential induction of cytokine genes and activation of mitogen-activated protein kinase family by soluble CD40 ligand and TNF in a human follicular dendritic cell line, J. Immunol. 163 (1999) 631–638.
[30] H. Shao, B. Wilkinson, B. Lee, P.C. Han, J. Kaye, Slow accumulation of active mitogen-activated protein kinase during thymocyte differentiation regulates the temporal pattern of transcription factor gene expression, J. Immunol. 163 (1999) 603–610.
[31] T. Kubo, T. Ibusuki, E. Saito, T. Kambe, Y. Hagiwara, Vascular mitogen-activated protein kinase activity is enhanced via angiotensin system in spontaneously hypertensive rats, Eur. J. Pharmacol. 372 (1999) 279–285.
[32] K.B. Reddy, J.S. Krueger, S.B. Kondapaka, C.A. Diglio, Mitogen-activated protein kinase (MAPK) regulates the expression of progelatinase B (MMP-9) in breast epithelial cells, Int. J. Cancer 82 (1999) 268–273.
[33] A. Zetser, E. Gredinger, E. Bengal, p38 mitogen-activated protein kinase pathway promotes skeletal muscle differentiation participation of the MEF2C transcription factor, J. Biol. Chem. 274 (1999) 5193–5200.
[34] M. Haneda, T. Sugimoto, R. Kikkawa, Mitogen-activated protein kinase phosphatase: a negative regulator of the mitogen-activated protein kinase cascade, Eur. J. Pharmcol 365 (1999) 1–7.
[35] T.L. Yue, J. Ni, A.M. Romanic, J.L. Gu, P. Keller, C. Wang, S. Kumar, G.L. Yu, T.K. Hart, X. Wang, Z. Xia, TL1, a novel tumor necrosis factor-like cytokine, induces apoptosis in endothelial cells Involvement of activation of stress protein kinases (stress-activated protein kinase and p38 mitogen-activated protein kinase) and caspase-3-like protease, J. Bio. Chem. 274 (1999) 1479–1486.
[36] E. Drenkard, Antimicrobial resistance of Pseudomonas aeruginosa biofilms, Microbes Infect. 5 (2003) 1213–1219.
[37] T. Rasamiravaka, Q. Labtani, P. Duez, M.E. Jaziri, The formation of biofilms by pseudomonas aeruginosa: a review of the natural and synthetic compounds interfering with control mechanisms, Biomed. Res. Int. (2015) 759348.
[38] M. Bredel, I.F. Pollack, The p21-Ras signal transduction pathway and growth regulation in human high-grade gliomas, Brain Res. Rev. 29 (1999) 232–249.
[39] H. Ozawa, S. Shioda, K. Dohi, H. Matsumoto, H. Mizushima, C.J. Zhou, H. Funahashi, Y. Nakai, S. Nakajo, K. Matsumoto, Delayed neuronal cell death in the rat hippocampus is mediated by the mitogen-activated protein kinase signal transduction pathway, Neurosci. Lett. 262 (1999) 57–60.
[40] M. Gagiano, D. Van Dyk, F. Bauer, F.F. Lambrechts, M.G. Pretorius, Msn1p/Mss10p, Mss11p and Muc1p/Flo11p are part of a signal transduction pathway downstream of Mep2p regulating invasive growth and pseudohyphal differentiation in Saccharomyces cerevisiae, Mol. Microbiol. 31 (1999) 103–116.
[41] I. Dumler, A. Kopmann, A. Weis, O.A. Mayboroda, K. Wagner, D.C. Gulba, H. Haller, Urokinase activates the Jak/Stat signal transduction pathway in human vascular endothelial cells, Arterioscler. Thromb. Vasc. Biol. 19 (1999) 290–297.
[42] S. Ahn, S. Maudsley, L.M. Luttrell, R.J. Lefkowitz, Y. Daaka, Src-mediated tyrosine phosphorylation of dynamin is required for β2-adrenergic receptor internalization and mitogen-activated protein kinase signaling, J. Biol. Chem. 274 (1999) 1185–1188.
[43] M. Fenton, A.J. Sinclair, Divergent requirements for the MAPKERK signal transduction pathway during initial virus infection of quiescent primary B cells and disruption of Epstein-Barr virus latency by phorbol esters, J. Virol. 73 (1999) 8913–8916.
[44] E.G. Ignatova, M.M. Belcheva, L.M. Bohn, M.C. Neuman, C.J. Coscia, Requirement of receptor internalization for opioid stimulation of mitogen-activated protein kinase: biochemical and immunofluorescence confocal microscopic evidence, J. Neurosci. 19 (1999) 56–63.
[45] D.D. Browning, N.D. Windes, D.Y. Richard, Activation of p38 mitogen-activated protein kinase by lipopolysaccharide in human neutrophils requires nitric oxide-dependent cGMP accumulation, J. Biol. Chem. 274 (1999) 537–542.
[46] G. Liao, G. Kreitzer, T.A. Cook, G.G. Gundersen, A signal transduction pathway involved in microtubule-mediated cell polarization, FASEB J. 13 (1999) 257–260.
[47] T.P. Garrington, G.L. Johnson, Organization and regulation of mitogen-activated protein kinase signaling pathways, Curr. Opin. Cell Biol. 11 (1999) 211–218.
[48] J. Egea, C. Espinet, J.X. Comella, Calcium influx activates extracellular-regulated kinase/mitogen-activated protein kinase pathway through a calmodulin-sensitive mechanism in PC12 cells, J. Biol. Chem. 274 (1999) 75–85.
[49] A.R. Brasier, The NF-κB regulatory network, Cardiovasc. Toxicol 6 (2006) 111–130.
[50] M. Caivano, P. Cohen, Role of mitogen-activated protein kinase cascades in mediating lipopolysaccharide-stimulated induction of cyclooxygenase-2 and IL-1β in RAW264 macrophages, J. Immunol. 164 (2000) 3018–3025.
[51] L. Smerdová, J. Svobodova, M. Kabátkova, J. Kohoutek, D. Blazek, M. Machala, J. Vondracek, Up-regulation of CYP1B1 expression by inflammatory cytokines is mediated by the p38 MAP kinase signal transduction pathway, Carcinogenesis 35 (2014) 2534–2543.
[52] X. Song, H.M. Sheppard, A.W. Norman, X. Liu, Mitogen-activated protein kinase is involved in the degradation of p53 protein in the bryostatin-1-induced differentiation of the acute promyelocytic leukemia NB4 cell line, J. Biol. Chem. 274 (1999) 1677–1682.
[53] J. Wu, J. Li, Y. Cai, Y. Pan, F. Ye, Y. Zhang, Y. Zhao, S. Yang, X. Li, G. Liang, Evaluation and discovery of novel synthetic chalcone derivatives as anti-inflammatory agents, J. Med. Chem. 54 (2011) 8110–8123.
[54] R. You, W. Long, Z. Lai, L. Sha, K. Wu, X. Yu, Y. Lai, H. Ji, Z. Huang, Y, Discovery of a potential anti-inflammatory agent: 3-oxo-29-noroleana-1, 9(11), 12-trien-2, 20-dicarbonitrile, J. Med. Chem. 56 (2012) 1984–1995.
[55] G.A. O'Toole, R. Kolter, Initiation of biofilm formation in Pseudomonas fluorescens WCS365 proceeds via multiple, convergent signalling pathways: a genetic analysis, Mol. Microbiol. 28 (1998) 449–461.
[56] S.Y. Hwang, J.H. Shin, J.S. Hwang, S.Y. Kim, J.A. Shin, E.S. Oh, S. Oh, J.B. Kim, J.K. Lee, I.O. Han, Glucosamine exerts a neuroprotective effect via suppression of inflammation in rat brain ischemia/reperfusion injury, Glia 58 (2010) 1881–1892.